Global and Planetary Change 217 (2022) 103947

Contents lists available at ScienceDirect

Global and Planetary Change

journal homepage: www.elsevier.com/locate/gloplacha

Research article

Paleoceanography of the Northwestern Greenland Sea and Return Atlantic Current evolution, 35–4 kyr BP

Dhanushka Devendra [a,*], Magdalena Łącka [a], Maciej M. Telesiński [a], Tine L. Rasmussen [b], Kamila Sztybor [c], Marek Zajączkowski [a]

[a] Department of Paleoceanography, Institute of Oceanology, Polish Academy of Sciences, Sopot 81-712, Poland
[b] CAGE-Centre for Arctic Gas Hydrate, Environment and Climate, Department of Geosciences, UiT The Arctic University of Norway, Tromsø, Norway
[c] Akvaplan-Niva AS, Framsenteret, 9296 Tromsø, Norway

ARTICLE INFO

Editor: Dr. Fabienne Marret-Davies

Keywords:
Fram Strait
Atlantic Water
Foraminifera
Stable isotopes
Late Weichselian

ABSTRACT

The flow of the Atlantic Water (AW) via the Return Atlantic Current (RAC) regulates the oceanographical conditions in the Northwestern (NW) Greenland Sea in the Fram Strait. As the intensity of the RAC might significantly influence both deep-water formation in the area and the stability of the Northeast Greenland Ice Sheet (NE GIS), knowledge of its variability in the past is important. Here we present a reconstruction of the paleoceanographic forcing of the AW on climatic conditions and associated environmental changes in the NW Greenland Sea by means of foraminiferal assemblages, stable (oxygen and carbon) isotopes, and various sedimentological parameters from sediment core GR02-GC retrieved from NE Greenland continental slope (1170 m water depth). Our data indicate an almost continuous presence of AW in the NW Greenland Sea during the last 35 kyr BP. Two peaks of low planktic $\delta^{18}O$ values at ~34.5 and 33 kyr BP are interpreted as meltwater signals associated with warm AW-induced melting of the adjacent NE GIS. The NE GIS advanced between 32 and 29 kyr BP, resulting in reduced meltwater influx to the NW Greenland Sea. Increased iceberg calving and melting after 29 kyr BP, were probably linked to surface warming and glacier advance to the shelf-break lasting until 23.5 kyr BP. During the Last Glacial Maximum, the extensive sea ice cover was associated with the presence of subsurface AW at the study site. During the Bølling–Allerød (B/A, ~14.6–12.7 kyr BP) strong melting of glaciers and sea ice was probably caused by the combined effect of the B/A warming and the flow of warm AW. The RAC was weakened during the Younger Dryas (~12.8–11.7 kyr BP), which reduced the advection of warm AW to the NW Greenland Sea. After 11.7 kyr BP, the RAC reached its modern strength, whereas, during the Holocene Thermal Maximum, it reached its maximum strength for the study period. In addition, short-term weakening of AW inflow to the core site was observed, especially at 10.5, 8.5, and 5.8 kyr BP.

1. Introduction

The NW Greenland Sea in the Fram Strait plays an important role as the main gateway for the deep and surface water exchange between the Arctic and North Atlantic Ocean. The region is very sensitive to climate and ocean circulation changes because of the East Greenland Current (EGC; Fieg et al., 2010), which carry sea ice and cold, low-salinity surface water from the Arctic Ocean, and thus regulate deep-water formation in the area (Håvik et al., 2017; Rudels and Quadfasel, 1991). The northward transport of Atlantic Water (AW) from the North Atlantic Current (NAC) to the Arctic Ocean in the eastern Fram Strait (Fig. 1) is an integral element in regulating the climate system in the Northern Hemisphere. About half of the northward propagating AW recirculates in the Fram Strait (de Steur et al., 2014; Hattermann et al., 2016) and afterward enters the NW Greenland Sea as Return Atlantic Water (RAW) via the Return Atlantic Current (RAC) (Jeansson et al., 2008; Paquette et al., 1985) (Fig. 1). The remaining half continues to flow northward into the Arctic Ocean and recirculates in the Eurasian and Canadian basins, where it is cooled and freshened to become Arctic Atlantic Water (AAW) (Fig. 1) (Rudels et al., 2012). Through these recirculation patterns, these waters join the EGC and flow further south to the North Atlantic along the eastern Greenland continental shelf (Bashmachnikov et al., 2021; Rudels et al., 2012) (Fig. 1). Furthermore, the stability of the NE Greenland Ice Sheet depends on the amount of warm AW delivered

* Corresponding author.
E-mail address: devendra@iopan.pl (D. Devendra).

https://doi.org/10.1016/j.gloplacha.2022.103947
Received 7 May 2022; Received in revised form 15 August 2022; Accepted 6 September 2022
Available online 10 September 2022
0921-8181/© 2022 The Authors. Published by Elsevier B.V. This is an open access article under the CC BY license (http://creativecommons.org/licenses/by/4.0/).

by the RAC (Schaffer et al., 2017).

Recent studies have focused on the paleoceanography of the EGC over the NE Greenland shelf covering the last c. 13 kyr (e.g., Davies et al., 2022; Pados-Dibattista et al., 2022; Syring et al., 2020a); however, only a few multi-proxy studies of the AW flux over a longer time period exist (Bauch et al., 2001; Ezat et al., 2021; Fronval and Jansen, 1997; Spielhagen and Mackensen, 2021). Thus, the Late Glacial and deglacial evolution of this AW flux is mostly unknown. The AW has been continuously present in the eastern part of the Nordic Seas (Rasmussen and Thomsen, 2008) and in the eastern Fram Strait (Rasmussen et al., 2007) during the last 24 kyr, despite the collapse of the AMOC during the Heinrich Stadial 1 (H1) (McManus et al., 2004). However, during the cold stadial events of H1 and the Younger Dryas, AW in the eastern Nordic Seas propagated as a subsurface water mass below the polar surface water layer (Ślubowska-Woldengen et al., 2007). The AMOC was reinvigorated at the onset of the Bølling-Allerød interstadials and led to an increase in the northward inflow of AW, resulting in deep-water renewal in the Nordic Seas. Studies from the eastern Fram Strait (e.g., Rasmussen et al., 2007; Werner et al., 2016) have previously demonstrated that the NAC was strengthened during the Early Holocene due to maximum summer insolation and thermohaline circulation, which increased heat advection to the Arctic Ocean. In certain studies in the Svalbard region (e.g., Rasmussen et al., 2014), ocean temperatures were shown to be higher than for the rest of the Holocene with a much warmer Mid-Holocene and probable greater heat transfer to the Arctic Ocean.

The present study aims to investigate variations in the properties and flow of the AW, especially from the RAC and associated changes over the NE Greenland margin during the last ~35 kyr BP by a multi-proxy study of benthic and planktic foraminiferal faunas, stable isotopes, ice-rafted debris (IRD), and other geochemical and sedimentological proxies. To produce a more comprehensive account of the changes in AW routing during the Late Weichselian glaciation and Holocene in the NW Greenland Sea, we also compare our records from GR02-GC (underlying the EGC) with a published record from a site (JM10-335GC) in the eastern Fram Strait (79°00.173N, 6°55.335E, 1197 m water depth; Sztybor and Rasmussen (2017)) directly underlying the northward flowing West Spitsbergen Current (WSC) directly derived from the NAC (Fig. 1). More importantly, this study offers the first detailed reconstruction of the evolution of the RAC, ~35–4 kyr BP.

2. Regional settings

The NE Greenland continental shelf is known to be the broadest shelf along the Greenland margin, reaching up to 300 km at its widest point. It is bordered by the East Greenland coastline to the west, the continental slope reaching down to 4000 m depth to the east, and the Fram Strait to the northeast. The shelf is characterized by five conspicuous cross-shelf troughs carved by former ice streams between shallow banks (Arndt et al., 2015). There are three major marine-terminating glaciers of the NE Greenland Ice Sheet that drain in the area, namely the Nioghalvfjerdsfjorden Glacier (or 79G), Storstrømmen and Zachariæ Isstrøm, which extends approximately 700 km inland (Joughin et al., 2001).

Our core site, located on the plateau on the continental slope of NE Greenland (~20 km east of the shelf-break), lies beneath the flow path of the southward flowing EGC (Johannessen, 1986). The EGC transports sea ice from the Arctic Ocean year-round, resulting in extreme sea-ice conditions on the NE Greenland shelf and upper slope throughout the year. Due to its origin in the Arctic Ocean, as well as seasonal ice melt in the Nordic Seas and Fram Strait, the Polar surface layer of the EGC is cold (−1.5 °C) and contains a large amount of freshwater (Rudels et al., 2002). Summer insolation makes the upper few meters of the surface layer warmer, but the temperature rapidly drops below that.

The EGC contains three distinct branches; the Polar Surface Water jet (PSW jet) on the shelf, shelf-break EGC in the vicinity of the shelf-break, and outer EGC over the continental slope (Håvik et al., 2017). The PSW jet transports mostly Polar Water, and during the summertime, it may be strengthened due to the freshwater runoff from the Greenland Ice Sheet (GIS). The outer EGC contains the warm subsurface RAW (Håvik et al., 2017), derived from the western branch of the WSC in the Fram Strait and transported via the RAC (Jeansson et al., 2008). AAW also flows southward along with the EGC as a subsurface water mass. The AAW, which enters from the Arctic Ocean is relatively cold (T: ≥ 0 °C), the RAW forms the warmest AW part of the EGC (T: ≥ 2 °C) (e.g., Rudels

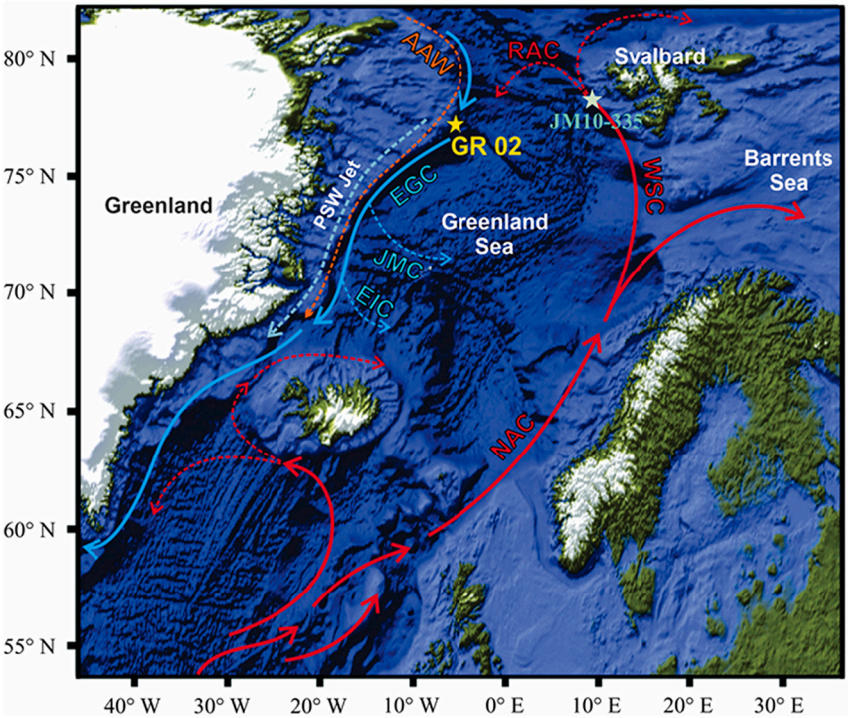

Fig. 1. (a) Schematic of present-day surface ocean circulation in the Nordic Seas. The red arrows represent the flow of warm Atlantic Water, i.e., North Atlantic Current (NAC), West Spitsbergen Current (WSC), and Return Atlantic Current (RAC). Blue arrows denote East Greenland Current (EGC) along the continental shelf break. Arctic Atlantic Water (AAW) flow from the Arctic is indicated by orange dashed arrows. Blue dashed arrows represent Jan Mayen Current (JMC) and East Icelandic Current (EIC). Light blue dashed arrow represents the Polar Surface Water jet (PSW jet). Yellow star indicates core location of gravity core GR02-GC (this study). White star indicate gravity core JM10-335GC discussed in the text (Sztybor and Rasmussen, 2017). (For interpretation of the references to colour in this figure legend, the reader is referred to the web version of this article.)

et al., 2002). The extensive eddy activity promotes the westward propagation of the RAW in the northern part of the Fram Strait and it combines with the shelf-break EGC (Hattermann et al., 2016).

3. Materials and methods

Gravity core GR02-GC was retrieved from the NW Greenland Sea (77°05.192 N, 5°13.896 W, 1170 m water depth) during the AREX expedition with RV Oceania in summer 2017 (Fig. 1). The water column temperature and salinity at the coring site were measured in situ by a mini-CTD (conductivity–temperature–depth) profiler at intervals of 1 s. After sediment core opening, the visual description was performed and colour information obtained based on the Munsell Soil Colour Chart (Fig. 3). The sediment core consists of grayish fine-grained mud and pale orange/brownish sandy mud and apparently represents continuous sedimentation with no sign of redeposition. The 1.35 m long core was sliced at 0.5 cm intervals, freeze-dried, and wet sieved over 63 μm, 100, and 500 μm.

3.1. AMS-^{14}C dates and chronology of core GR02-GC

For the construction of the age model, specimens of the planktic foraminifera *Neogloboquadrina pachyderma* were picked from 9 horizons for AMS ^{14}C dating (Table 1;¸ five dates were previously published by Telesiński et al. (2022)). The resulting raw radiocarbon dates were calibrated to calendar ages using the CALIB ^{14}C software (8.2.0; Stuiver et al. (2022)) and the Marine20 dataset (Heaton et al., 2020), and no local reservoir correction was applied (ΔR = 0 years). The age model for core JM10-335GC from the eastern Fram Strait (Fig. 1) was created from existing ^{14}C dates on *N. pachyderma* (Sztybor and Rasmussen, 2017) and recalibrated using Marine20, applying a local reservoir correction (ΔR = 7 ± 11) (Mangerud et al., 2006). We are well aware of the statement of Heaton et al. (2020) that Marine20 is inaccurate in higher latitudes, where variations in sea-ice extent, Polar water, ocean upwelling, and air-sea gas exchange may have caused changes in the reservoir age. However, since our core site is on the slope and strongly influenced by the RAW, we are confident that changes in reservoir ages through time match changes in other North Atlantic records (e.g., Brendryen et al., 2020). Therefore, in this study, we used the Marine20 dataset to calibrate radiocarbon ages for both cores GR02-GC and JM10-335GC (Table 1).

The age obtained in GR02-GC at 50.5 cm is older than the age at 54.5 cm (Table 1). This age reversal was possibly caused by reworking of older speciemns of *N. pachyderma* to the site, and the older date was therefore excluded from the age model. The age at 24.5 cm, we have excluded as being too young and used the age at 10.5 cm to build the age model (Table 1). This is based on the percentage distribution of *C. wuellerstorfi* (an almost strictly interglacial species) (e.g., Bauch, 1997; Haake and Pflaumann, 1989) and the pattern of sedimentation rates (see Supplementary Fig. 1A, B). Using the age at 24.5 cm and discarding the age at 10.5 cm would give sedimentation rates of 18.4 cm kyr^{-1} between 24.5 and 6.5 cm (between 11 and 10 kyr BP; unusually high for records from >1000 m water depth in the Fram Strait (e.g., Nørgaard-Pedersen et al., 2003). Accepting the age at 10.5 cm for the age model, we calculated the highest sedimentation rates (12.5 cm kyr^{-1}) to occur between 40.5 and 10.5 cm (between 16.45 and 14.05 kyr BP; see Supplementary Fig. 1A). Sedimentation rates in the Nordic Seas were usually high during the deglaciation due to melting of the ice sheet margins and increase in iceberg discharge (e.g., Nørgaard-Pedersen et al., 2003).

The calculation of the age-depth model was done using linear interpolation between dating points. All ages are given in thousand calendar years before 1950 CE (kyr BP).

3.2. Micropaleontological analyses

Ninety-three sediment samples in total were analyzed from core GR02-GC for foraminiferal, ice-rafted debris (IRD), and stable isotope analyses. When possible, a minimum of 300 benthic and 300 planktic foraminiferal specimens from the >63 μm fraction of each sample were picked under the light microscope and mounted on faunal slides. However, a few samples (five samples between 118 and 128 cm) had only few specimens present. Only samples containing at least 50 specimens were included for calculations. When necessary, residues were split using a dry micro splitter, and the total number of foraminifera was calculated. The taxonomic classification was performed mostly to species level, using the generic classification of Loeblich Jr and Tappan (2015). The absolute abundance of individuals for each sample was calculated as number of individuals per 1g dry sediment [# g^{-1}]. Relative abundances were calculated as a percentage of total individuals

Table 1
AMS ^{14}C measurements and calibrated ages applying the Marine20 calibration curve.

Lab ID	Depth (cm)	Dated material	^{14}C age (year BP)	Calibrated age (year BP, 2σ)		
				Min age	Max age	Median age
Core GR02-GC						
OS-147528	2.5	*N. pachyderma*	5350 ± 20	5361	5661	**5524**
OS-151013	3.5	*N. pachyderma*	5790 ± 20	5871	6171	**6006**
OS-147529	6.5	*N. pachyderma*	9330 ± 30	9774	10,154	**9975**
OS-140812	10.5	*N. pachyderma*	12,600 ± 110	13,696	14,497	**14,050**
OS-151014	24.5	*N. pachyderma*	10,050 ± 40*	Excluded		
OS-140813	40.5	*N. pachyderma*	14,300 ± 460	15,261	17,631	**16,450**
OS-147508	44.5	*N. pachyderma*	20,200 ± 360	22,563	24,146	**23,354**
OS-147509	50.5	*N. pachyderma*	25,100 ± 390*	Excluded		
OS-140814	54.5	*N. pachyderma*	22,800 ± 270	25,655	26,837	**26,169**
OS-140815	86.5	*N. pachyderma*	25,700 ± 430	28,145	29,953	**29,071**
OS-140816	134.5	*N. pachyderma*	31,600 ± 1100	32,871	37,887	**35,271**
Core JM10-335GC						
(Sztybor and Rasmussen, 2017)	20	*N. pachyderma*	9302 ± 38	9700	10,129	**9800**
(Sztybor and Rasmussen, 2017)	56	*N. pachyderma*	10,829 ± 43	11,832	12,363	**12,055**
(Sztybor and Rasmussen, 2017)	75	*N. pachyderma*	11,830 ± 44	12,985	13,306	**13,140**
(Sztybor and Rasmussen, 2017)	278	*N. pachyderma*	15,486 ± 73	17,653	18,192	**17,941**
(Sztybor and Rasmussen, 2017)	290	*N. pachyderma*	16,830 ± 71	19,095	19,681	**19,409**
(Sztybor and Rasmussen, 2017)	369	*N. pachyderma*	19,327 ± 77	22,141	22,697	**22,385**
(Sztybor and Rasmussen, 2017)	460	*N. pachyderma*	27,132 ± 150	30,106	30,830	**30,440**

Median ages (in bold) were used for the age-depth model. Calibrated ages are reported in thousand years before 1950 CE (kyr BP).
* The radiocarbon ages from 24.5 and 50.5 cm were excluded from the age–depth model (described in Section 3.1).

(planktic and benthic foraminifera were treated separately). Part (15–4 kyr BP) of planktic foraminifera analysis have been published by Telesiński et al. (2022).

The fluxes of planktic and benthic foraminifera were calculated for all the counted samples, using foraminiferal number (FN) [# g^{-1}], linear sedimentation rate (LSR) [cm yr^{-1}], and dry bulk density (DBD) [g cm^{-3}]. The LSR was calculated by using the calibrated ages. The foraminiferal fluxes were calculated by using the following formula:

Flux (individuals × cm^{-2} × kyr^{-1}) = FN × DBD × LSR.

3.3. Stable isotopes, IRD, and grain sizes

For stable carbon and oxygen isotope analysis, approximately 10 specimens of the planktic foraminiferal species *Neogloboquadrina pachyderma* and 25 specimens of the benthic species *Cassidulina neoteretis* were picked from the 100–500 μm size fraction. All samples were cleaned in methanol, and measurements were performed using a Thermo Finnigan MAT 252 mass spectrometer with a Kiel III automatic carbonate preparation device at the Light Stable Isotope Mass Spec Laboratory, Department of Geological Sciences, University of Florida, USA. Measurement precision was better than ±0.04‰ and ± 0.02‰ for oxygen and carbon isotopes, respectively. The obtained data are given in the usual δ notation, referring to the Peedee Belemnite (PDB) standard. The $\delta^{18}O$ values for *C. neoteretis* were corrected for vital effects by 0.02‰ and $\delta^{13}C$ values by 1.5‰ (Poole et al., 1994). Part (15–4 kyr BP) of the stable isotope analyses ($\delta^{18}O$ and $\delta^{13}C$) of *N. pachyderma* and *C. neoteretis* have been published by Telesiński et al. (2022).

For IRD content counts of grains larger than 500 μm in 85 samples were performed. The number of IRD/g dry weight sediment was calculated. The flux was calculated, using the absolute abundance of IRD [# g^{-1}], linear sedimentation rate (LSR) [cm yr^{-1}], and dry bulk density (DBD) [g cm^{-3}].

The grain-size distribution was measured in 68 samples by a laser particle analyzer, Mastersizer2000 (Malvern) at the Institute of Oceanology, Poland, and grouped into three fractions, sand, silt, and clay (<63 μm).

3.4. Organic bulk sediment parameters

Total carbon (TC) and total organic carbon (TOC) were measured on homogenized bulk sediment samples using the combustion technique with chromatographic detection, performed with a Flash 2000 elemental analyzer by Thermo. The TOC measurements were performed after removing residual carbonate by adding hydrochloric acid. The carbonate content ($CaCO_3$) was calculated according to TOC and TC values, using the following equation.

$$CaCO_3 = (TC - TOC) \times 100/12$$

4. Results

4.1. CTD and water masses

The presented temperature and salinity data in Fig. 2a are limited to the upper 300 m due to the instrument's limitations. In order to show the changes in temperature and salinity below the 300 m depth, we plotted the data set from Boyer et al. (2018) (Fig. 2b). However, Fig. 2b does not represent the exact bottom temeperature below 1000 m water depth due to the interpolation of the limited available data.

The upper layer of the water column over the NE Greenland shelf consists of low saline (~29 psu) and cold (~ −1.5 °C) Polar Water (PW) from the Arctic Ocean below a layer of local meltwater (Fig. 2a). As the coring site (GR02-GC) is located >200 km from the Northeast Greenland Ice Sheet (NE GIS), the local surface water layer is ~15 m thick with a temperature of ~2 °C (Fig. 2). The PW is typically 150–200 m thick over the shelf (Fig. 2), and thins out to 50 m further offshore (Håvik et al., 2017). The water mass below the PW at our site is of Atlantic origin and occupies the depth below ~150 m (Fig. 2a, T > 2 °C; S > 35.5 psu).

4.2. Lithology and grain size

Four informal lithological units (L1–L4) were identified in core GR02-GC (Fig. 3). The base of the core, (L1,135–118 cm) contains homogeneous brownish grey silty clay-rich mud (Fig. 3). The lower-mid section (L2, 118–60 cm) is characterized by homogenoeous light grey coarse-grained sandy sediment with large drop stones in the upper part of the unit (Fig. 3); also a high content of IRD is observed throughout the unit (Fig. 3). The upper section (L3, 60–5 cm) is characterized by homogenoeous grayish brown sediment of clay and silt with drop stones at the base, middle and top of the unit (Fig. 3). The top part of the core (L4, 5–0 cm) is characterized by fine grayish yellow brown sediment with very low IRD content (Fig. 3).

4.3. Age model

The age model indicates that the 135 cm long sediment core covers the last ~35.3 kyr BP (Fig. 3). The maximum sedimentation rate of core

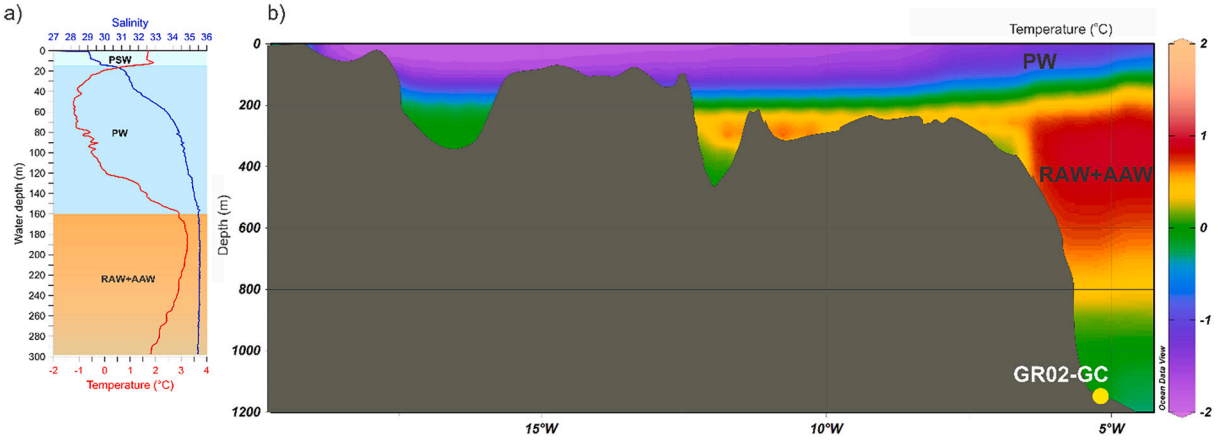

Fig. 2. (a) CTD (Conductivity, temperature, depth) profile measured in August 2017 at the core site of GR02-GC (temperature (red line) and salinity (blue line)). Main water masses are marked. (b) Water column temperature in the upper 1200 m measured along a transect at 77.25° N showing the main water masses at the study site of GR02-GC. Yellow circle indicates location of coring site. Abbreviations: Polar Water (PW), a combination of Return Atlantic Water (RAW) and Arctic Atlantic Water (AAW). Temperature data from World Ocean Atlas 2018 (Boyer et al., 2018). (For interpretation of the references to colour in this figure legend, the reader is referred to the web version of this article.)

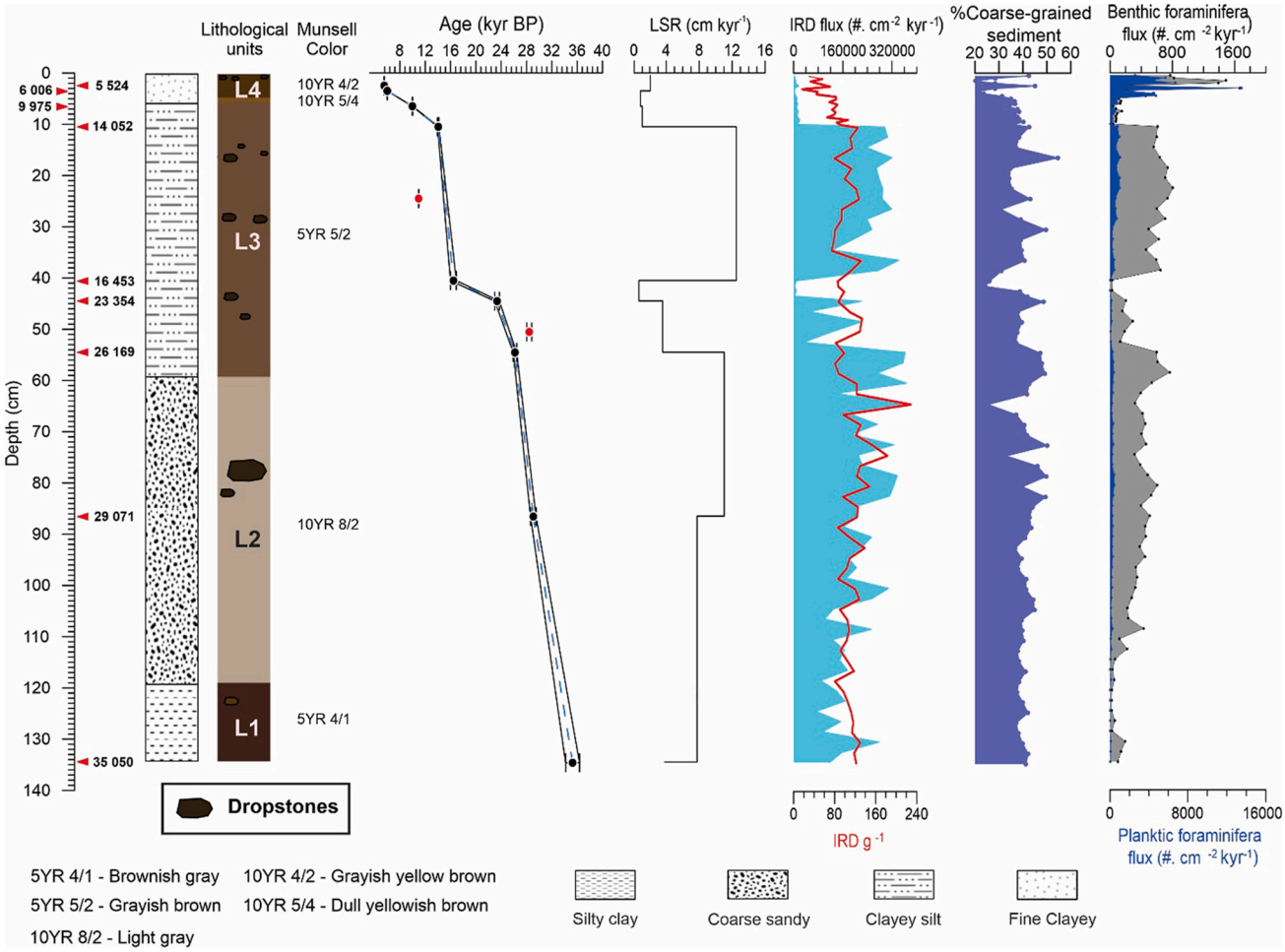

Fig. 3. Lithological log with Munsell colour codes, age-depth model (two red dots indicate dates excluded from the age model), linear sedimentation rates (LSR), ice-rafted debris (IRD) flux (upper scale) and IRD absolute abundance (lower scale), percentage of coarse fraction (>63 μm), benthic foraminiferal flux (upper scale), and planktic foraminiferal flux (lower scale) of core GR02-GC. Red triangles indicate dating points with calibrated ages BP. (For interpretation of the references to colour in this figure legend, the reader is referred to the web version of this article.)

GR02-GC, 12.51 cm kyr^{-1} is recorded between 16.45 and 14.05 kyr BP (Fig. 3). The sedimentation rate is extremely low during the Last Glacial Maximum (LGM).

4.4. Foraminiferal faunas

A total of 58 benthic foraminiferal species and four planktic species were identified. Most of the specimens of both benthic and planktic foraminifera were well-preserved with minor or no signs of dissolution of the tests. The concentration varies in general between 1 and 491 individuals (ind.) g^{-1} sediment (sed.) throughout the core (Fig. 4). On average, benthic calcareous foraminifera account for 99% of the total benthic foraminiferal assemblages. The ten most abundant benthic foraminiferal species are *Cassidulina neoteretis* (4–77%), *Cassidulina reniforme* (5–43%), *Cibicides lobatulus, Cibicidoides wuellerstorfi* and *Astrononion hamadaense* (also called *Astrononion gallowayi*) (0–27%), *Elphidium clavatum* (0–27%), *Cribroelphidium albiumbilicatum* (0–25%), *Oridorsalis umbonatus* (0–14%), *Islandiella norcrossi* (0–9%), and *Buccella frigida* (0–9%). The relative abundances of *C. reniforme* show an inverse relationship to *C. neoteretis* throughout the core.

The dominant planktic foraminiferal species in the entire core is the polar species *N. pachyderma* (~53–94%), followed by the subpolar species *Turborotalita quinqueloba* (~6–40%). The maximum abundance and flux of the planktic foraminifera occurred in the mid-Holocene (8–4.5 kyr BP) (Fig. 5).

The distribution of foraminiferal species is relatively uniform throughout the core, with highest variability in the lower 134–60 cm (lithological units L1 and L2). In the upper part (the Holocene, lithological unit L4), *C. neoteretis*, *C. wuellerstorfi*, *M. barleeanus*, *N. labradorica* and *O. umbonatus* increase in relative abundance, while *C. reniforme*, *I. norcrossi* and *B. frigida* decrease gradually. *Stainforthia loeblichi* is absent.

In the following, we divide the results into foraminiferal zones (FZ) defined by major changes in sedimentation rates and fluxes of planktic and benthic foraminifera, indicating potential changes in the environment (Figs. 4 and 5).

4.4.1. FZ I – 134.5-114.5 cm; 35.2–32.5 kyr BP

This foraminiferal zone is characterized by a low benthic foraminiferal flux (average 66 ind. cm^{-2} kyr^{-1}) and concentration (average 4 ind. g^{-1} sed.) with low but highly variable flux of IRD. The benthic assemblage is dominated by *E. clavatum,* that fluctuates slightly throughout the zone. There are two distinct peaks in *C. neoteretis* at ~45% and 35% at ~34.2 and 33.4 kyr BP, respectively (Fig. 4). This coincides with peaks in *C. lobatulus* and *A. hamadaense.* The abundance of *C. reniforme* and *I. norcrossi* decrease toward the top of the zone.

4.4.2. FZ II – 114.5-46.5 cm; 32.5–23.5 kyr BP

The benthic calcareous assemblage is dominated by *C. reniforme* (average 28%), *C. neoteretis* (average 24%), and *E. clavatum* (average 11%), but of high variability (Fig. 4). This interval is characterized by high sedimentation rates, as well as high IRD and benthic foraminiferal

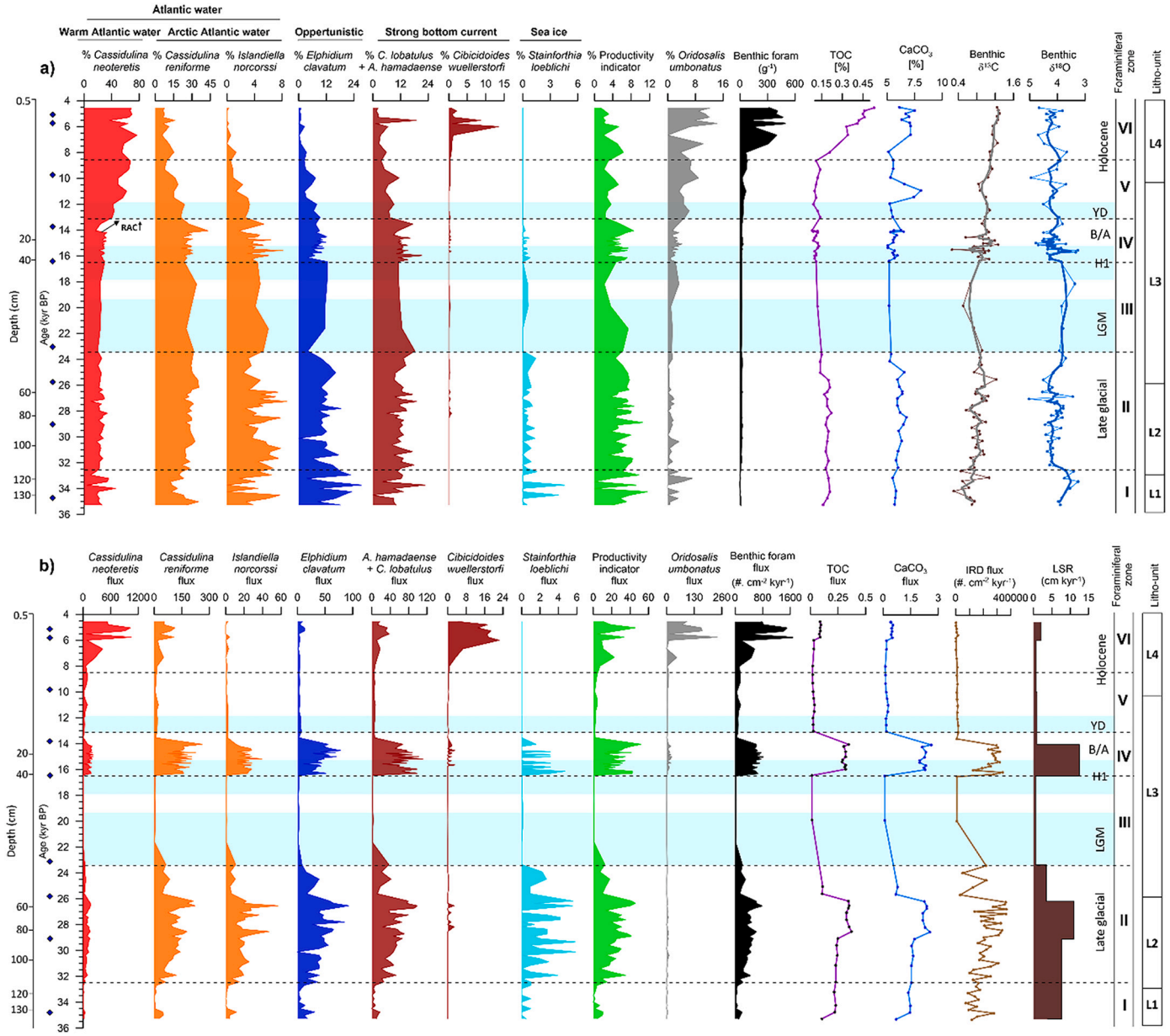

Fig. 4. Panel (a): Relative abundances (shadings) of selected benthic foraminiferal species and their ecological preferences (see text for explanation). Atlantic water (AW) group: warm AW indicator species – *Cassidulina neoteretis (red shading); AAW indicators* – *Cassidulina reniforme* and *Islandiella norcrossi* (orange shading); unstable bottom conditions indicator – *Elphidium clavatum* (blue shading); bottom current indicators - *Cibicides lobatulus,* and *Astrononion hamadaense* added together, and *Cibicidoides wuellerstorfi*; productivity indicators – *Buccella frigida, Melonis barleeanus and Nonionellina labradorica* (green shading); sea-ice cover indicator – *Stainforthia loeblichi* (light blue shading); low-productivity indicator - *Oridorsalis umbonatus* (Grey shading); absolute abundance of benthic foraminiferal (black shading); total organic carbon (%TOC; purple line) and calcium carbonate (%$CaCO_3$*; blue line); benthic foraminiferal* $\delta^{13}C$ and $\delta^{18}O$ (3-point moving average of isotope records shown in thick dark lines). Panel (b): Fluxes (shadings) of selected benthic foraminiferal species; total flux of benthic foraminifera (black shading); total organic carbon flux (purple line); calcium carbonate flux (blue line); ice rafted debris (IRD) flux (brown line); linear sedimentation rates (LSR). Foraminiferal zones (zone I–VI) and lithological units are shown on the right side of the panels. Black diamonds next to the left y-axis indicate radiocarbon dates. Abbreviations: LGM - Last Glacial Maximum; H1 - Heinrich Stadial 1; B/A - Bølling-Allerød; YD - Younger Dryas. (For interpretation of the references to colour in this figure legend, the reader is referred to the web version of this article.)

(BF) fluxes, which range between 766.7 and 120 ind. cm^{-2} kyr^{-1} (Fig. 4). The TOC content is relatively high (~0.25%; Fig. 4). The planktic assemblage is dominated by *N. pachyderma* in the entire zone (Fig. 5). Between 34 and 33 kyr BP, subpolar species show relatively high abundance.

4.4.3. FZ III- 46.5-41.5 cm; 23.5–16.5 kyr BP

In this foraminiferal zone, sedimentation rates are very low and data points few. However, we recognize a benthic calcareous assemblage still dominated by *C. reniforme* (average 30%), *C. neoteretis* (average 24%), and *E. clavatum* (average 10%) (Figs. 4). *S. loeblichi* is exceedingly rare near the base of the zone; it first appeared at 20.5 kyr BP and then was present the top of the zone. Benthic foraminiferal and planktic fluxes are low (63 and 43 ind. cm^{-2} kyr^{-1}, respectively). The IRD flux decreases significantly (Fig. 4).

4.4.4. FZ IV – 41.5-9.5 cm; 16.5–12.8 kyr BP

In foraminiferal zone IV, planktic and benthic foraminiferal fluxes

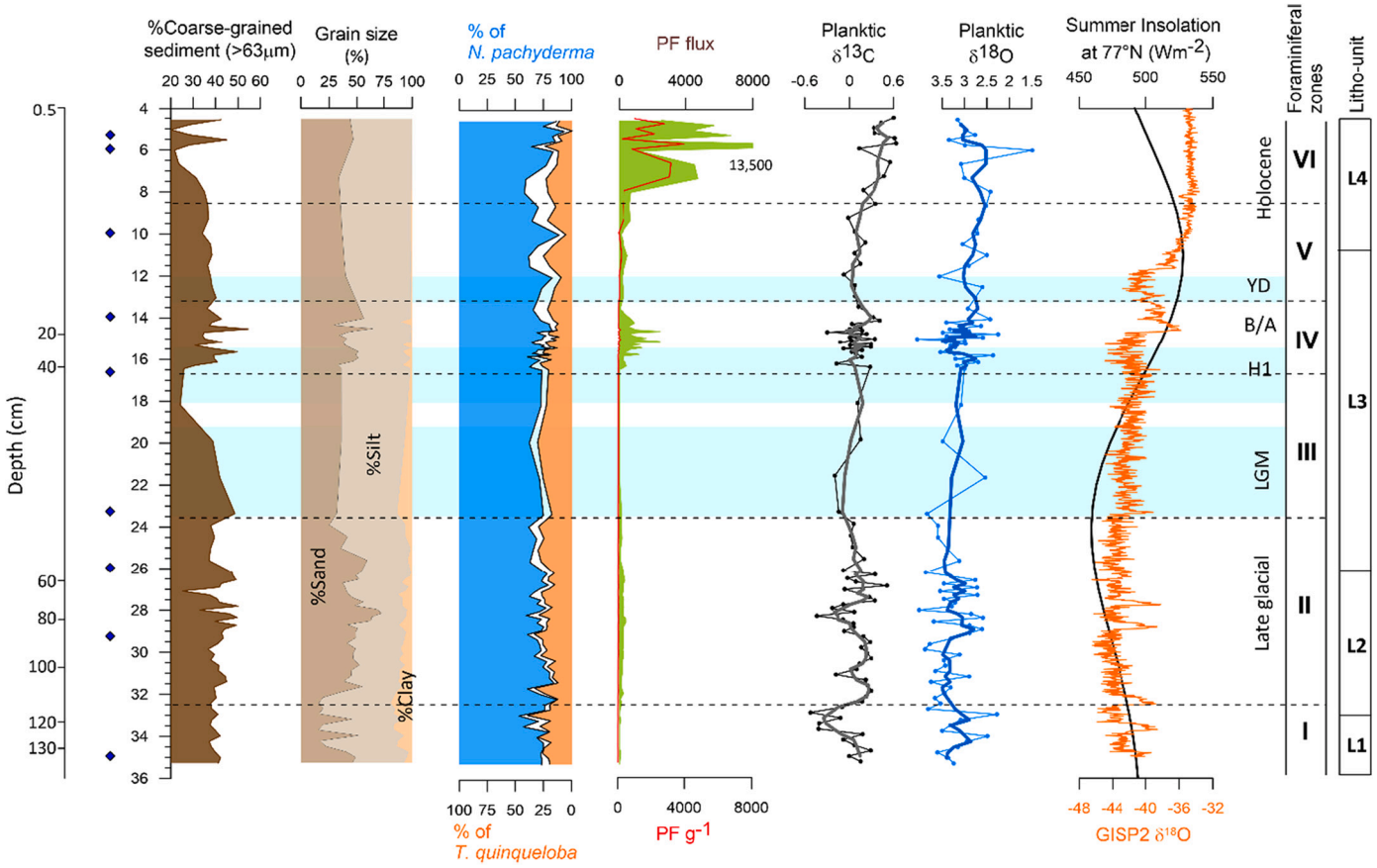

Fig. 5. Planktic foraminiferal data, grain sizes, and isotopes and correlation of core GR02-GC to the GISP2 ice core. Percentage of coarse-grained sediments (>63 μm), grain size distribution, percentage of polar species *Neogloboquadrina pachyderma* and subpolar species *Turborotalita quinqueloba*, total planktic foraminiferal (PF) fluxes, and abundance, summary of the planktic foraminiferal stable isotopes ($\delta^{13}C$ and $\delta^{18}O$) records (3-point moving average of isotope records shown in thick dark lines), summer insolation at 77°N (black line) and $\delta^{18}O$ of GISP2 ice core (orange line) (Grootes et al., 1993). Black diamonds next to the left y-axis indicate radiocarbon dates. Foraminiferal zones (zone I–VI) and lithological units are shown to the right. Abbreviations: LGM - Last Glacial Maximum; H1 - Heinrich Stadial 1; B/A - Bølling-Allerød; YD - Younger Dryas.

show higher values than in the previous zone (average 388 and 230 ind. cm^{-2} kyr^{-1}, respectively). The abundance of *C. neoteretis* (average 28%) drops noticeably at 14 kyr BP to 16%, while *C. reniforme* shows a sudden increase up to maximum value for the entire core (~45%) (Fig. 4). The flux of IRD (~370 × 10^3 grains cm^2 kyr^{-1}) is the highest recorded within the core. The TOC content increases at the end of the interval.

4.4.5. FZ V - 9.5-5.5 cm; 12.8–8.5 kyr BP

Foraminiferal zone V is dominated by *C. neoteretis* (average 54%), followed by *C. reniforme* (average 16%) and *C. lobatulus* (average 6%). In the lower part, *C. neoteretis* shows a sudden increase (from 16% to 43% at 12.8 kyr BP), while *C. reniforme* shows a distinctive drop (from 43% to 21%) (Fig. 4). *Cibicidoides wuellerstorfi* is absent in the lower part (Fig. 4). The IRD flux shows a relatively low value. The %TOC is fairly stable throughout the zone, but a rapid increase of $CaCO_3$ is observed between 12 and 10 kyr BP.

4.4.6. FZ VI – 5.5-0.5 cm; 8.5–4.5 kyr BP

This zone is strongly dominated by *C. neoteretis* (average 62%), followed by *C. reniforme* (average 9%). The % of *I. norcrossi* and *E. clavatum* decreases, while *C. wuellerstorfi* increases. A peak in % of *C. lobatulus* plus *A. hamadaense is* observed at 5.5 kyr BP. The planktic and benthic foraminiferal concentrations are the highest in the entire record. At the base of the zone (~8.5–7 kyr BP), the % of planktic *N. pachyderma* decrease, and % subpolar *T. quinqueloba* increase. The TOC content gradually increases to the maximum of the entire record at the end of the interval.

4.5. Stable isotopes

The $\delta^{18}O$ values in *N. pachyderma* vary between 1.49‰ and 4.05‰, with an average of 3.16‰. The $\delta^{13}C$ of *N. pachyderma* vary between −0.52‰ and 0.63‰, with an average $\delta^{13}C$ of 0.12‰ (Fig. 5).

The $\delta^{18}O$ and $\delta^{13}C$ values of *C. neoteretis* are shown in Fig. 4. Except for the LGM interval, similar patterns in planktic and benthic $\delta^{18}O$ values are displayed. Benthic $\delta^{13}C$ values follow the benthic $\delta^{18}O$ in the lower part of the core (35–25 kyr) and change toward lower values during the LGM.

5. Discussion

5.1. Ecological significance of selected benthic and planktic foraminifera

Within the sub-polar North Atlantic, *C. neoteretis* is most abundant in areas fed by warm and saline AW underneath cold and low salinity Polar surface waters (Cage et al., 2021; Jennings and Helgadottir, 1994; Jennings and Weiner, 1996; Jennings et al., 2004; Seidenkrantz, 1995) (Fig. 4). Therefore, we interpret dominance of this species as indicating presence of warm saline subsurface AW in the northern Greenland Sea. To identify the relative contribution of AW from the Arctic Ocean (AAW), we use the AAW species (also known as chilled-AW species), including *C. reniforme* (Hald and Korsun, 1997; Sejrup et al., 1981) and *I. norcrossi* (Jennings et al., 2004; Korsun and Polyak, 1989; Mudie et al., 1984). *Cassidulina reniforme* can live in somewhat colder water masses than *I. norcrossi* (Ślubowska-Woldengen et al., 2007). *Elphidium clavatum*

has been previously linked to low bottom water temperature, low salinity, high turbidity, and we use this species as an indicator of unstable conditions at the bottom (Hald and Vorren, 1987; Korsun and Hald, 1998; Łącka and Zajączkowski, 2016; Steinsund, 1994). We consider *B. frigida, M. barleeanus* and *N. labradorica* as indicators for increased productivity and flux of organic matter to the sea floor (Hald and Steinsund, 1996; Steinsund, 1994; Wollenburg and Kuhnt, 2000). *M. barleeanus* has also been linked to partly degraded organic carbon in the sediment (Caralp, 1989; Fontanier et al., 2002). *Stainforthia loeblichi* has been reported to thrive in areas of seasonal sea-ice cover (Scott et al., 1984; Seidenkrantz, 2013; Steinsund, 1994) and we thus interpret *S. loeblichi* as an indicator of seasonal sea-ice cover or of presence of the sea-ice margin. *Oridorsalis umbonatus* is a deep-sea species most abundant in the western Nordic Seas and Arctic Ocean under dense sea-ice cover and very low food supply (Wollenburg and Mackensen, 1998). *Cibicides lobatulus* and *A. hamadaense* are current indicator species, with the latter attracted to higher productivity than the former (Wollenburg and Mackensen, 1998). *Cibicidoides wullerstorfi* is also living in areas of strong bottom currents in low-food conditions (Mackensen et al., 1985). This species is mostly found in interglacial conditions in North Atlantic records and is typical in Holocene sediments (Haake and Pflaumann, 1989).

The subpolar planktic foraminiferal species *T. quinqueloba* has been linked to the advection of warm AW in the modern western Fram Strait (Pados and Spielhagen, 2014; Volkmann, 2000). The polar species *N. pachyderma* indicates presence of cold and fresh polar surface water and likely extensive sea-ice cover (Greco et al., 2019; Pados and Spielhagen, 2014; Simstich et al., 2003). In conclusion, we interpret *T. quinqueloba* as associated with AW, whereas *N. pachyderma* is associated with cold Polar water.

5.2. Paleoenvironmental reconstruction

5.2.1. FZ I, 35.2–32.5 kyr BP – less productive harsh environment

The low foraminiferal fluxes, low planktic $\delta^{13}C$ and slightly low TOC content point to low surface water productivity. Peaks relative abundances of both *S. loeblichi* and *O. umbonatus,* indicate extensive sea-ice cover over the NE Greenland shelf and slope, in support of the interpretation of low productivity. Colder surface water conditions could promote the sea-ice cover where ice-core data indicate that the mean annual temperature was generally similar as during the LGM (Rasmussen et al., 2013). The high relative abundance of the opportunistic benthic foraminiferal species *E. clavatum* suggests the environmental conditions were unfavorable for other foraminiferal species, probably due to the lower bottom temperatures and limited fresh food availability at the sea bottom. The presence of a productivity indicator species (*M. barleeanus*) could suggest a higher organic matter influx to the bottom. However, *M. barleeanus* prefers low-quality, more degraded organic matter (Caralp, 1989; Fontanier et al., 2002), suggesting reduction in the supply of fresh organic matter from surface primary production.

Our planktic $\delta^{18}O$ record shows two signals of low values at ~34.5 and 33.4 kyr BP, most likely due to high meltwater flux, presumably as a result of sudden warmings (correlating in time to the Dansgaard-Oescheger (D—O) warming events 5 and 6; Fig. 5), and/or presence of relatively warm AW at the subsurface, both of which promote glacial melting (Moros et al., 2002; Syvitski et al., 1996). We identified two pronounced peaks of the warm AW indicator, *C. neoteretis*, indicating two short periods of intensive inflow of warm AW to the site (Fig. 4). This is supported by the low benthic $\delta^{18}O$ values which is taken as a signal of warming of the bottom water (e.g., El bani Altuna et al., 2021; Ezat et al., 2014; Rasmussen et al., 1996), coinciding with the distinct drop in % of *E. clavatum* (Fig. 4). At the same time, peak relative abundance of current indicator species *C. lobatulus* and *A. hamadaense* (Fig. 4) coincide with peaks in % sand and coarse-grained sediments (Fig. 5), which suggests significant bottom currents connected to the EGC (Evans et al., 2002; Mienert et al., 1992). We propose that the primary source of the two meltwater signals recorded in the NW Greenland Sea was the advection of warm subsurface waters to the ice sheet margin, which resulted in enhanced melting, as it does today (Håvik et al., 2017; Schaffer et al., 2020; Schaffer et al., 2017). This subsurface warming correlate in time with southeastern Nordic Seas records showing strong (sub)surface warming and inflow of AW (Rasmussen and Thomsen, 2008).

5.2.2. FZ II, 32.5–23.3 kyr BP – dynamic interaction of AW and induced changes in NE GIS

This interval is characterized by high sediment flux, high IRD flux, and deposition of coarse-grained lithofacies, likely due to the advance of NE GIS onto the continental shelf toward the shelf edge (Figs. 4 and 5). This is in agreement with the previous findings of high sedimentation rates and IRD flux in response to the Late Weichselian advance of eastern GIS onto the continental shelf (e.g., Evans et al., 2002). The AW indicator species (mostly AAW) and the opportunistic species *E. clavatum* are dominant, indicating a strong input of AW to our core location but also unstable and cold bottom conditions. The presence of Atlantic-derived water at times caused higher surface productivity, seen as small peaks in the relative abundance of the productivity-indicator species, high BF flux and high %TOC, implying increased organic matter input to the sea floor (Fig. 4). The comparatively high planktic $\delta^{13}C$ values also indicate enhanced surface water productivity through most of the interval (Fig. 5). However, the dominance of *N. pachyderma* in the planktic assemblages indicates the presence of cold polar surface water and likely extensive sea-ice cover (Greco et al., 2019). The latter is also supported by the increased, yet very variable flux of *S. loeblichi* that usually thrives in areas of seasonal sea-ice cover (Seidenkrantz, 2013).

From 32.5 kyr BP to ~29 kyr BP, both benthic and planktic $\delta^{18}O$ were relatively high (Figs. 4 and 5), suggesting a likely expansion of the NE GIS. Similar to this, Larsen et al. (2010) documented shelf-based ice build-up in the northernmost Greenland shelf nearly at 30 kyr BP. Both BF and PF fluxes increased (Figs. 4 and 5), indicating enhanced surface water productivity, further supported by high planktic $\delta^{13}C$ and relatively high abundances of the productivity indicator species *B. frigida* and *M. barleeanus* (Fig. 4). This was most likely associated with an influx of nutrient-rich AAW, as indicated by increase in % *C. reniforme* (Fig. 4).

At 29–26 kyr BP planktic $\delta^{18}O$ decrease, IRD deposition and sedimentation rates increase indicating meltwater discharge and likely retreat of the NE GIS (Figs. 4 and 5). A comparatively high (approximately 30%) abundance of the subpolar planktic species *T. quinqueloba* indicates relatively warm (sub)surface water as a likely trigger for glacier melting (Fig. 5). This interpretation is also supported by a relatively high percentage of the opportunistic *E. clavatum,* indicating a high-turbidity environment possibly due to the sediment-laden meltwater (Corliss, 1991; Hald et al., 1994; Łącka and Zajączkowski, 2016).

After 26 kyr BP, lower sedimentation rates and decreased IRD flux and increased planktic $\delta^{18}O$ (Figs. 4 and 5), indicate cooling and reduced glacier melting. Previous studies also reported that NE GIS advanced after 26 kyr BP toward the shelf edge or to its LGM position (Arndt et al., 2017; Evans et al., 2009; Larsen et al., 2018). At the same time, the % of AW-indicator species together decline slightly, while the sea-ice indicator *S. loeblichi* increases, reflecting an increase in sea-ice formation and slight weakening of advection of AW (Fig. 4). The presence of sea ice has also been observed in the Fram Strait during this time interval (Müller et al., 2009). The %TOC and planktic $\delta^{13}C$ decrease indicating low primary production in the surface water (Figs. 4 and 5). The gradual increase in % of bottom current indicators suggests stronger bottom currents after 26 kyr BP. On the lower NE Greenland continental slope, debris-flow deposits changed into episodic turbidity current activity, which was then modified into sediment waves by contourite bottom currents (Cofaigh et al., 2004; Evans et al., 2009). Therefore, we propose that NE GIS extended to the near-shelf edge at 23.5 kyr BP, marking the onset of the LGM.

5.2.3. FZ III, 23.5–16.5 kyr BP – continuous inflow of AW

The interpretation is problematic due to the comparatively low temporal resolution caused by extremely low sedimentation rates (0.56 cm kyr^{-1}) and thus very few data points (Figs. 4 and 5). However, the trend from the previous time interval 26 – ~24 kyr BP of cooling with some influence of AW is indicated by the continuous presence of the AAW indicator species. The similar continuous flux of AW to the NE Greenland shelf during this period was also reported by Rasmussen et al. (2022). In addition, the very low foraminiferal fluxes coincide with extremely low sedimentation rate and low IRD flux (Fig. 4), suggesting the presence of extensive sea-ice cover at the NE Greenland shelf during the LGM and early deglaciation. This near-permanent sea-ice cover, especially during the LGM and early deglaciation is also reported in a records from the NE Greenland shelf (Rasmussen et al., 2022) and Fram Strait (Müller et al., 2009).

Between ~18.5 and 16.5 kyr BP, the abundance of AAW indicator species decreased while the abundance of warm AW indicator species increased marginally (Fig. 4), indicating increased advection of warm AW (see also Section 5.3) compared to the LGM. The slight decrease in benthic $\delta^{18}O$ also suggest comparatively warm bottom conditions possibly due to the expansion of the warm AW. This is in accordance with recent findings of the presence of warm AW at the NE Greenland shelf (Rasmussen et al., 2022). The % of the planktic foraminifera *N. pachyderma* increases slightly and indicates presence of cold, polar surface water (Fig. 5). The productivity indicator species tend to decline, indicating lower surface water productivity than during the LGM (Fig. 4). An increase in sea-ice cover than the LGM, as indicated by the presence of sea-ice indicator species, could explain the drop in productivity.

5.2.4. FZ IV; 16.5–12.8 kyr BP – rapid retreat of NE GIS augmented by warming and AW inflow

Planktic $\delta^{18}O$ values are relatively low between 16.5 and 15 kyr BP (Fig. 5). Low planktic $\delta^{18}O$ is a regional feature of the deglaciation at the Greenland continental margin (Evans et al., 2002; Nam et al., 1995), indicating cold and relatively fresh surface water conditions, which may cause surface stratification (de Vernal et al., 2005; Rudels, 1989). The flux of IRD and sedimentation rates are high, implying landward retreat of the NE GIS and more iceberg rafting. Evidence of a similar rapid retreat with similar timing is reported in the NE GIS (Arndt et al., 2017) and the Barents Sea and Fennoscandian ice sheets (Lekens et al., 2005; Rørvik et al., 2010). Intense deglacial iceberg rafting at the outer NE Greenland shelf has also been reported by previous studies by ploughmarks on the shelf (Arndt et al., 2017; Rasmussen et al., 2022). A relatively high % of current indicator species during this period is suggested to indicate the presence of strong, probably cold bottom currents (Fig. 4). A high peak in % of coarse-grained sediments (Fig. 5) also indicates bottom conditions more favorable for the current indicator species *C. lobatulus*, which dominates in areas of coarse sediments (Mackensen et al., 1985).

The Bølling-Allerød warm interstadial (B/A, ~14.8–12.9 kyr BP) is also associated with decreased planktic $\delta^{18}O$ and elevated deposition of IRD (Figs. 4 and 5), implying unstable oceanographic conditions influenced by meltwater influx. Stronger bottom current activity is suggested by a high peak in % of the current indicator species, coarse-grained sediments and high % sand content (Figs. 4 and 5). The onset of the B/A and retreat and melting of the NE GIS and associated increase in sedimentation rates, is correlated in time with the melting of the Svalbard-Barents Sea Ice Sheet (Lubinski et al., 2001; Mangerud et al., 1992; Vorren and Kristoffersen, 1986). The composition of the benthic foraminiferal faunas north off Svalbard (Ślubowska et al., 2005) and in the south-western Barents Sea (Aagaard-Sørensen et al., 2010) indicates the progressive inflow of warm AW through the Fram Strait and into the Barents Sea during the B/A. We suggest that this noticeable glacier-melting induced freshwater event in the Nordic Seas and Barents Sea was a combined effect of the rapid warming of the B/A (higher $\delta^{18}O$ in the GISP2 record (Grootes et al., 1993), Fig. 5) and warm-AW induced glacier and sea-ice melting. Predominantly sea-ice free surface conditions at the Fram Strait also support our interpretation of sea ice melting (Müller et al., 2009). This combined effect probably accelerated the rate of glacier retreat and the subsequent major meltwater pulse, which caused a sea-level rise during the B/A (Carlson and Clark, 2012; Deschamps et al., 2012; Fairbanks, 1989). The retreat of the GIS margin from the shelf and coast during this interval was documented by numerous previous studies (Carlson et al., 2008; Cofaigh et al., 2004; Larsen et al., 2010; Möller et al., 2010; Ó Cofaigh et al., 2013).

The conditions were unstable indicated by the highly variable benthic and planktic $\delta^{18}O$ and $\delta^{13}C$ and increase in % of *E. clavatum* (Figs. 4 and 5). A relatively high abundance of the productivity indicator species and generally high BF and PF fluxes and high planktic $\delta^{13}C$ (Fig. 4) suggest high primary production in the surface water. The supply of terrigenous material from the melting probably supplemented the nutrient levels in the upper surface water masses (Knies and Stein, 1998).

5.2.5. FZ V; 12.8–8.5 kyr BP – dynamic environment with the progressive inflow of AW

Although the resolution is relatively low, at ~12.6 kyr BP low planktic $\delta^{18}O$ can be observed (Fig. 5), probably corresponding to the cold Younger Dryas stadial (YD, ~12.8–11.7 kyr BP). The AMOC was partially weakened during the YD, in contrast to the temporary shutdown during H1 (McManus et al., 2004), which significantly reduced the northward intrusion of warm AW. According to Łącka et al. (2020), a large area of the Nordic Seas was affected by freshwater during the YD. The presence of AW indicators (Fig. 4) suggests that when AMOC declined, the AW could still reach the site at the sea floor. At the same time, the surface was cold, as indicated by a peak in % of *N. pachyderma* (Fig. 5). Therefore, we suggest that during the YD, the NE Greenland shelf was influenced by AW probably at the subsurface. This is in agreement with findings from the inner shelf of NE Greenland (Davies et al., 2022; Jackson et al., 2022), north of Iceland (Knudsen et al., 2004), and in the northern Baffin Bay (Knudsen et al., 2008), where the AW was observed as a subsurface water mass.

Immediately after the YD, there was a noticeable rise in the relative abundance of warm-AW indicators, pointing to a strong advection of warm AW at least until 10.5 kyr BP (Fig. 4). The surface water temperatures also started to increase as suggested by the gradual increase of subpolar species (Fig. 5), possibly due to the expansion of the warm AW. Relatively high meltwater supply at this time is supported by relatively low planktic $\delta^{18}O$ and $\delta^{13}C$ values (Fig. 5). Peaks of $CaCO_3$ and productivity indicator species coincide with low IRD flux suggesting enhanced biological productivity and strongly reduced sea-ice cover. Similar conditions were also reported for the NE Greenland inner shelf (Syring et al., 2020b) and Fram Strait (Müller et al., 2012) during the early Holocene. After a short period of weakening of the inflow of warm AW and surface cooling seen by a decrease in *C. neoteretis* and high percentages of *N. pachyderma* (~10.5–9.5 kyr BP) (Fig. 5), a short-lasting recovery occurred until ~8.5 kyr BP. The decrease in warm AW indicators and replacement by AAW indicator species suggests relatively cold AAW still present at our site. Similarly, previous studies also observed a continuous but variable influx of AW toward the NE Greenland shelf after YD, at least until 8.5 kyr BP (Davies et al., 2022; Rasmussen et al., 2022; Syring et al., 2020a; Zehnich et al., 2020).

5.2.6. FZ VI; 8.5–4.5 kyr BP – development of highly productive environment

The surface cooling at ~8.5 kyr BP was previously observed on the NE Greenland shelf (Syring et al., 2020a) and eastern Nordic Seas (Husum and Hald, 2012; Risebrobakken et al., 2011). Our results show that the propagation of warm AW undergoes a short decline between 8.5 and 7.5 kyr BP, as indicated by a relatively low abundance of warm AW indicators (Fig. 4). However, relatively high surface water temperatures

are indicated by a high % *T. quinqueloba* and drop of % *N. pachyderma* (Fig. 5). Our suggestion of relatively weaker warm AW flow at ~8.5–7.5 kyr BP is in accordance with the recent findings from the NW Greenland Sea (Davies et al., 2022; Pados-Dibattista et al., 2022; Syring et al., 2020b).

The peak in % *C. neoteretis* (~ 80%) together with a peak in *C. lobatulus* plus *A. hamadaense* and *C. wuellerstorfi* (warm AW indicator and bottom current species, respectively) at ~7.5–5.5 kyr BP indicates the strongest intrusion of warm AW to our site. Concurrently, the glaciomarine environment indicator species *E. clavatum* decreases noticeably. This probably marks the maximum strength of warm AW inflow to the NW Greenland Sea during the last 35 kyr BP, and possibly correlates with an expansion of warm AW into the Nordic Seas under the Holocene Thermal Maximum (HTM) (Koç et al., 1993; Sarnthein et al., 1995). Extremely low sedimentation rates coincide with low IRD flux (Fig. 4) pointing to a low productivity of icebergs over the NE Greenland shelf (Davies et al., 2022). In this period, when the grounded glaciers were situated about 80 km further inland than it is today, indicates the time of minimal ice sheet extent (Bennike and Weidick, 2001). The maximum % of the almost exclusively interglacial species, *C. wuellerstorfi* indicates strong deep-water current activity, similar to the modern conditions on the deeper slopes of the Nordic Seas (Hald and Steinsund, 1992; Mackensen et al., 1985). Davies et al. (2022) and Syring et al. (2020b) found evidence of reduced AW intrusion to the NE Greenland inner shelf were after 7.9 kyr BP. We suggest this discrepancy is due to the location of the studied sediment cores. The sediment cores collected closer to the coast were predominantly affected by meltwater/Greenland local water. Håvik et al. (2017) explained the modern oceanography of the NE Greenland shelf and concluded that the near-shore water mass is colder, quite distinct from the Atlantic-origin Water. Our core was collected almost below the outer EGC, which contains more warm AW than inner shelf EGC (Håvik et al., 2017). We propose that the southward flowing warm AW thus did not reach the NE Greenland inner shelf between ~7.5 and 5.5 kyr BP.

Around 5.2 kyr BP, our record shows a decrease in % *T. quinqueloba,* implying surface cooling, probably correlating in time with an increased sea-ice transport from the Arctic along the NE Greenland shelf (Andrews et al., 2009; Cabedo-Sanz et al., 2016; Pados-Dibattista et al., 2022; Syring et al., 2020b). Decreased warm AW inflow is supported by a reduction in warm-AW indicator species (Fig. 4) which correlates with the findings of Zehnich et al. (2020). A similar surface cooling was previously reported in records from the northeastern Nordic Seas (Łącka et al., 2019; Telesiński et al., 2014; Werner et al., 2013). Generally, high planktic and benthic foraminiferal fluxes, small peaks in relative abundance of the productivity-indicator species *M. barleeanus* and *N. labradorica* and increasing planktic $\delta^{13}C$ point to higher surface water productivity from ~8.5 to 4.6 kyr BP as also indicated by the increasing %TOC and %$CaCO_3$ (Fig. 4).

5.3. Flow of Return Atlantic Water into the Greenland Sea via RAC

The paleoceanographic interpretation based on the presented proxy records provides information about the flow of AW in the NW Greenland Sea. At the Greenland (Sheldon et al., 2016) and Svalbard margins (Jessen et al., 2010; Ślubowska-Woldengen et al., 2007; Ślubowska et al., 2005), the inflow of warm AW is generally linked to the retreat of the ice sheet since the Late Glacial. Here, we compare our results on the flow of AW into the NW Greenland Sea during the last ~35 kyr BP with a record from the eastern Fram Strait, core JM10-335GC (Sztybor and Rasmussen (2017) to better constrain the changes in the inflow of warm RAW on a regional basis (Fig. 6). In order to interpret warm RAW influx to our site, we use the difference in relative abundance between the warm AW indicator species (*C. neoteretis*) and AAW indicator species (*C. reniforme* and *I. norcrossi*). According to Rudels et al. (2002, 2005), the RAW forms the warmest part of the Atlantic Water of the EGC, while the AAW entering from the Arctic Ocean is considerably colder. Therefore, we assume that the balance between these two AW indicator groups predominantly reflects the weakening or strengthening of the AW influx through the RAC.

Data from core GR02-GC demonstrates the continuous presence of AW (warm RAW and/or AAW) in the NW Greenland Sea flowing beneath polar surface water during the last ~35–4 kyr (Fig. 7). The period between 35 and 14 kyr BP was predominantly dominated by AAW, with intervals of enhanced recirculation warm AW of the inflowing RAW to the NW Greenland Sea as discussed in below.

At ~34.5 and 33.4 kyr BP our records indicate warm AW signals possibly due to the strong influx of RAW to NE Greenland shelf via the strengthened RAC (Fig. 5). After 32.5 kyr BP, a strengthened WSC transport warm AW northward as recorded in core JM10-335GC, but the majority of the water enters the Arctic Ocean due to a weak RAC suggested by stable and low abundance of *C. neoteretis*. Increased abundance of the AAW indicator *C. reniforme* suggests relatively cold AAW influx to NW Greenland Sea from the Arctic Ocean. A noticeable decrease in % of *C. neoteretis* between 28.5 and 27 kyr in core JM10-335GC point to a significant reduction of northward propagation of AW through the WSC. A marginal but observable drop of *C. neoteretis* in our records was also observed possibly correlating with the reduced flux of warm RAW as a result of limited recirculation of the warm AW at the Fram Strait due to this weakening of WSC. The increase in relative abundance of *C. neoteretis* and subpolar *T. quinqueloba* after ~27 kyr BP in core JM10-335GC suggests an enhanced influx of AW along the western Svalbard margin via the WSC (see also Sztybor and Rasmussen (2017)) (Fig. 6). A similar northward inflow of AW has been observed in the southeastern Nordic Seas at ~27 kyr BP (Andersen et al., 1996; Rasmussen and Thomsen, 2008). The combined records of the faunal and geochemical data from GR02-GC demonstrate that the inflow of warm RAW to the NW Greenland Sea was still weak due to a limited recirculation in the Fram Strait. We propose that most of the northward propagating AW must have entered the Arctic Ocean and flowed back to the NW Greenland Sea as AAW, as suggested by the increased abundance of AAW indicators. An increased advection of the AW to the southern Yermark Plateau at this time interval support our interpretation (Nørgaard-Pedersen et al., 2003).

During the LGM, the warm-AW indicator *C. neoteretis* in core GR02-GC showed roughly the same pattern as in the preceding interval (Fig. 6), suggesting continuous weak RAW inflow to the NW Greenland Sea (Fig. 7). Earlier studies have reported that due to the significant reduction of the North Atlantic convection (Boyle and Keigwin, 1987), the NAC was significantly slower than at present (McManus et al., 2004; Piotrowski et al., 2005). However, the warm-AW indicator species in core JM10-335GC indicates presence of AW in the eastern Fram Strait during the LGM (Fig. 6). Sztybor and Rasmussen (2017) interpreted this high abundance of the AW-indicator species as a result of high seasonal productivity, supported by the high benthic and planktic foraminiferal fluxes (Fig. 6). Shortly after the LGM (~18.5 kyr BP), the RAC marginally strengthened again, inferring a strengthening of AW recirculation in the Fram Strait. Similarly, warm AW signals during the early deglaciation at the NW Greenland Sea were also observed by Rasmussen et al. (2022). Considering the high abundance of *C. neoteretis* and "Atlantic species" (not shown in this paper; see Sztybor and Rasmussen (2017)) after 18 kyr BP in core JM10-335GC (Fig. 6), it is possible to interpret the strengthening of the RAC due to enhanced recirculation of AW in the Fram Strait.

During the B/A, besides the gradual increase of warm-AW indicator species, there is also a decrease in planktic $\delta^{18}O$ observed in JM10-335GC (Fig. 6), suggesting enhanced northward advection of AW and associated ice melting. This period is also time-equivalent with the resumption of AMOC after a short shut-down phase during H1 (McManus et al., 2004). The recirculation of AW in the Fram Strait also accelerated, and RAC was re-activated, resulting in the advection of RAW to the NW Greenland Sea (Fig. 7).

Despite the generally high percentage of warm AW indicator species

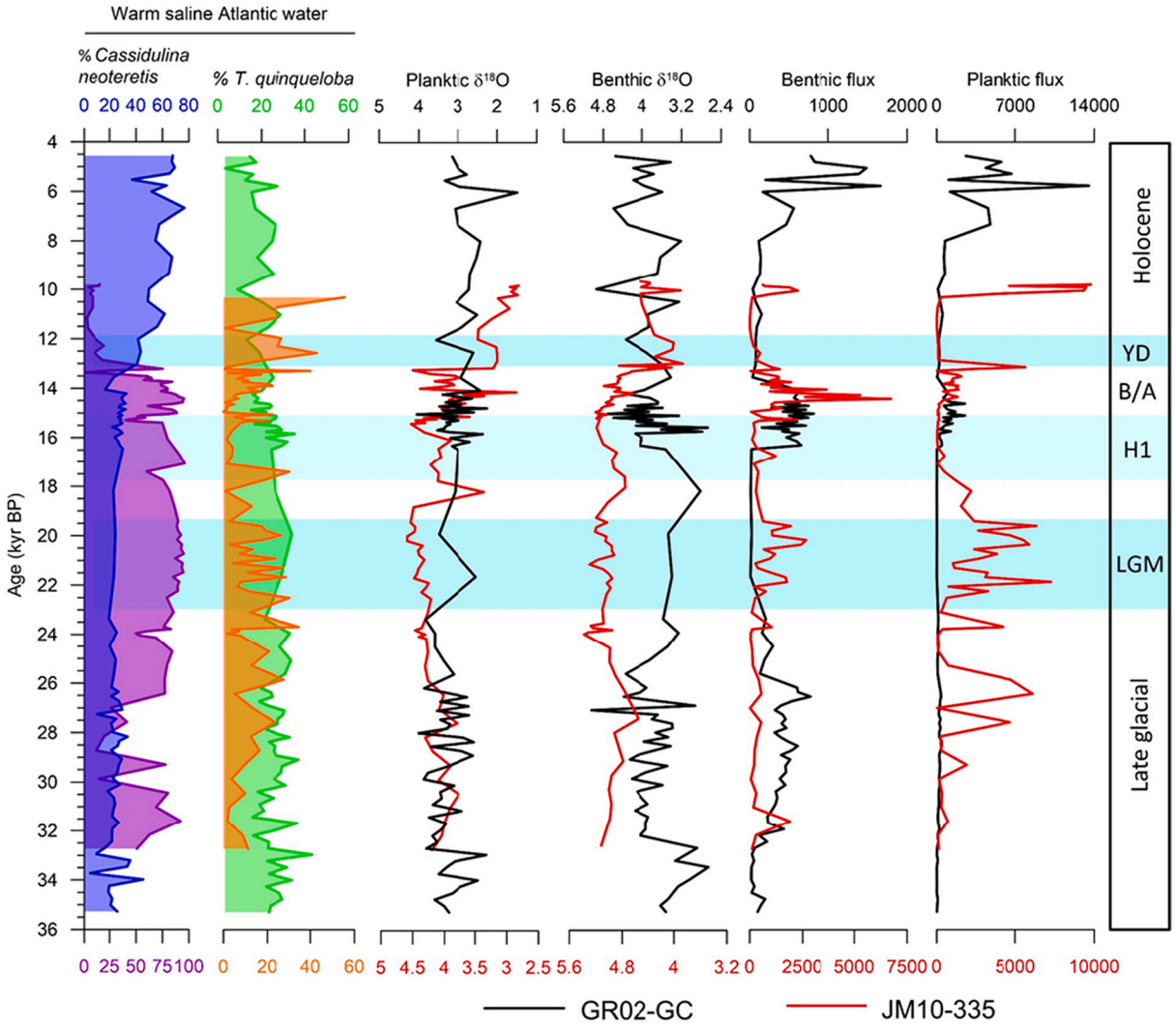

Fig. 6. Selected data from cores GR02-GC (black lines) and JM10-335GC (red lines): Relative abundance of benthic foraminiferal species *Cassidulina neoteretis* and planktic species *Turborotalita quinqueloba* in GR02-GC (blue and green shading, respectively) and JM10-335GC- (purple and orange shading, respectively)), planktic and benthic stable isotope records, and flux of benthic and planktic foraminifera. Abbreviations: LGM - Last Glacial Maximum; H1 - Heinrich Stadial 1; B/A - Bølling-Allerød; YD - Younger Dryas. (For interpretation of the references to colour in this figure legend, the reader is referred to the web version of this article.)

(>30%) throughout the last ~35–4 kyr BP in our records, the GR02-GC and JM10-335GC records demonstrate that a strong and permanent inflow of RAW from the eastern Fram Strait to the NW Greenland Sea began only after the B/A. This is indicated by the absolute dominance (>65%) and a gradual increase of the warm-AW indicator *C. neoteretis* from ~13 kyr BP onwards (Fig. 4). Our interpretation agrees well with previous findings from the NE Greenland shelf, where the warm AW signal also was found since ~13 kyr BP (Davies et al., 2022). Moreover, at the Svalbard margin (Rasmussen et al., 2007; Sarnthein et al., 1995; Telesiński et al., 2018) and the Barents Sea (Kristensen et al., 2013; Łącka et al., 2015), this major inflow of warm AW began at ~12.8 kyr BP. However, during the YD, the RAC weakened slightly due to the partially weakening of the AMOC (McManus et al., 2004), (Fig. 7). The weakening of northward advection of AW was also recorded in JM10-335GC, indicated by a drop in % *C. neoteretis* (Fig. 6). In contrast, Davies et al. (2022) and Jackson et al. (2022) observed advection of AW during the YD interval into the inner shelf of NE Greenland. However, the authors did not distinguish between the sources of paleo-Atlantic-source water and thus collectively refer to it as AW (combination of RAW and AAW). Our records also point to the presence of AW at our site, likely the majority is AAW as suggested by the high abundance of AAW indicator species. Therefore, we suggest that the NE Greenland shelf experienced a reduced influx of warm RAW via the RAC during the YD interval.

After the YD, the inflow of warm RAW increased dramatically due to reinvigoration of the RAC, marking the onset of the Holocene interglacial (~11.7 kyr BP) (Figs. 6 and 7). In the eastern Fram Strait, *T. quinqueloba* becomes abundant indicating AW was at the surface (Fig. 6). At NE Greenland shelf the decrease in AAW indicator species suggests dominance of warm RAW. Our records indicate that the reinvigoration of the RAC was more prominent than during the B/A (Fig. 6). Acceleration of the AMOC (McManus et al., 2004) and the abrupt Holocene warming (around 11.7 kyr BP) increased the recirculation of AW in Fram Strait and strengthened the RAC. After that, the acceleration of the RAC, and therefore the flow of warm AW to the NW Greenland Sea, continued to its modern strength (Fig. 7) but was interrupted slightly during short periods such as 10.5, 8.5, and 5.8 kyr BP (Fig. 4). This is in accordance with Zehnich et al. (2020), who reported strong, but the variable inflow of warm RAW until 5.6 kyr BP via the RAC to NE Greenland shelf. The enhanced AW recirculation in the Fram Strait and the maximum strength of the RAC observed at ~6.8 kyr BP possibly correlate with the HTM.

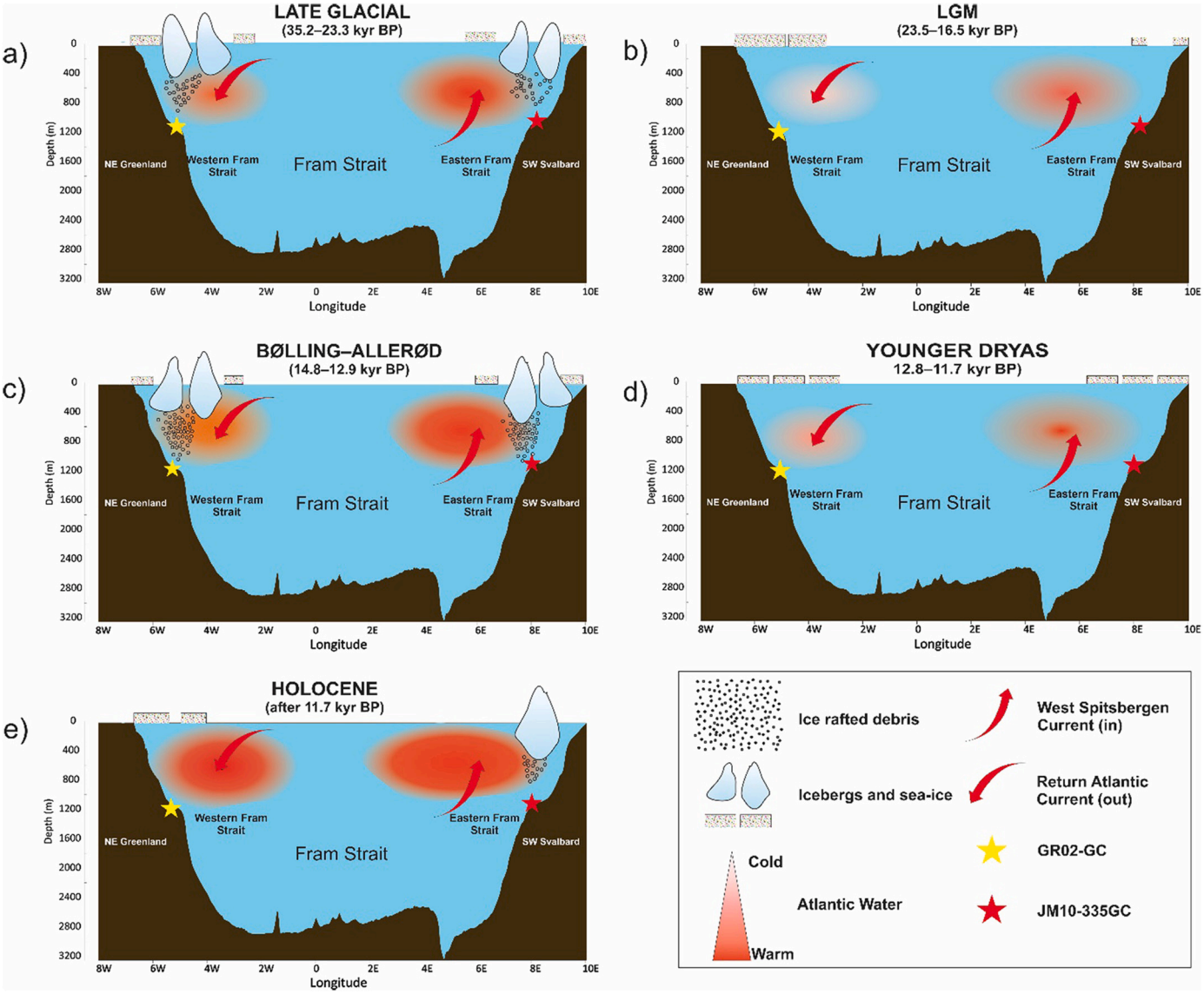

Fig. 7. Environmental conditions in western and eastern Fram Strait during, a) the Late Glacial, b) the Last Glacial Maximum (LGM), c) the Bølling-Allerød interstadials, (d) the Younger Dryas stadial, and (e) Holocene interglacial. Yellow stars mark the location of sediment core GR02-GC and red stars mark the location of JM10-335GC. (For interpretation of the references to colour in this figure legend, the reader is referred to the web version of this article.)

6. Conclusions

Our new multi-proxy record from the NW Greenland Sea reveals distinct paleoenvironmental changes in the interactions between AW being carried to the site and the response of the neighboring NE GIS over the Late Glacial and Holocene (35.3–4.6 kyr BP). The main conclusions of our study are described as follows:

- AW was continuously present in the NW Greenland Sea during the last 35 kyr BP.
- NW Greenland Sea was subjected to cold conditions in the Late Glacial interval (~ 35.3–23.3 kyr BP), possibly associated with extensive sea-ice cover and meltwater influx reinforced by melting the NE GIS. The progressive influx of warm AW to the region promoted glacier and sea-ice melting at 34.5 and 33.4 kyr BP similar to conditions near the glacier front today. In the latter part of the Late Glacial interval (after 26 kyr BP), warm AW advection was reduced, resulting in limited calving and melting.
- Although of low resolution, an extensive sea-ice cover was apparently present during the LGM. Sea ice became even more expansive after the LGM, significantly reducing the primary production at ~19–16.5 kyr BP.
- Evidence of an enhanced major meltwater pulse to the NW Greenland Sea is documented at the B/A (14.8–12.9 kyr BP), possibly associated with a combined effect of atmospheric warming during the B/A and warm AW-induced glacier and sea-ice melting. This meltwater supply increased the transport of freshly exposed post-glacial terrigenous material to the NW Greenland Sea, supplemented the nutrient levels in the upper surface water masses, causing increased primary production.
- Evidence of permanent strong inflow of warm AW via RAC to NW Greenland Sea began only after the B/A, reflected in absolute dominance of benthic foraminiferal warm AW-indicator species *Cassidulina neoteretis* from ~13 kyr BP. Short-lived weakening of the RAC occurred during the cold YD followed by a reinvigorated flow of AW up to modern strength during the Holocene with slight interruptions at short periods such as 10.5, 8.5, and 5.8 kyr BP.
- Warm AW stopped reaching the inner shelf of the NE Greenland shelf after ~7.5 kyr BP, but probably still reached the outer shelf.

Supplementary data to this article can be found online at https://doi.org/10.1016/j.gloplacha.2022.103947.

Data availability

All data presented in this paper are available at open database for Earth and Environmental Science PANGAEA (doi:https://doi.org/10.1594/PANGAEA.943502).

Author contributions

MZ planned the study; MZ, MŁ, and MMT collected the sediment core; MŁ performed grain size analysis; DD counted the IRD fraction; DD, MMT, and MŁ constructed the age-depth model; MŁ and MMT helped with the foraminifera analysis. DD, MZ, MMT, and MŁ wrote the manuscript draft. KSz and TLR provided data from core JM10-335GC. All authors contributed to data interpretation, writing and editing of the final manuscript.

Declaration of Competing Interest

The authors declare no competing interests.

Data availability

Data presented in this paper have been uploaded to PANGAEA (https://doi.org/10.1594/PANGAEA.943502)

Acknowledgments

The research was financially supported by the Norwegian Financial Mechanism for 2014-2021, project no 2019/34/H/ST10/00682. MZ and MŁ contribution was supported by National Science Centre in Poland through project 2019/33/B/ST10/00297. KSz and TLR received support from the Research Council of Norway through its Centers of Excellence funding scheme, grant number 223259, and UiT the Arctic University of Norway, Tromsø, Norway. We would like to thank Agnieszka Kujawa for picking and identifying the foraminiferal specimens. We also extend our gratitude to the R/V Oceania crew who helped during sediment core retrieval.

References

Aagaard-Sørensen, S., Husum, K., Hald, M., Knies, J., 2010. Paleoceanographic development in the SW Barents Sea during the Late Weichselian–Early Holocene transition. Quat. Sci. Rev. 29, 3442–3456.

Andersen, E.S., Dokken, T.M., Elverhøi, A., Solheim, A., Fossen, I., 1996. Late quaternary sedimentation and glacial history of the western Svalbard continental margin. Mar. Geol. 133, 123–156.

Andrews, J.T., Darby, D., Eberle, D., Jennings, A.E., Moros, M., Ogilvie, A., 2009. A robust, multisite Holocene history of drift ice off northern Iceland: implications for North Atlantic climate. The Holocene 19, 71–77.

Arndt, J.E., Jokat, W., Dorschel, B., Myklebust, R., Dowdeswell, J.A., Evans, J., 2015. A new bathymetry of the Northeast Greenland continental shelf: constraints on glacial and other processes. Geochem. Geophys. Geosyst. 16, 3733–3753.

Arndt, J.E., Jokat, W., Dorschel, B., 2017. The last glaciation and deglaciation of the Northeast Greenland continental shelf revealed by hydro-acoustic data. Quat. Sci. Rev. 160, 45–56.

Bashmachnikov, I.L., Fedorov, A.M., Golubkin, P.A., Vesman, A.V., Selyuzhenok, V.V., Gnatiuk, N.V., Bobylev, L.P., Hodges, K.I., Dukhovskoy, D.S., 2021. Mechanisms of interannual variability of deep convection in the Greenland Sea. Deep-Sea Res. I Oceanogr. Res. Pap. 174, 103557–103575.

Bauch, H.A., 1997. Paleoceanography of the North Atlantic Ocean (68–76 N) during the past 450 ky deduced from planktic foraminiferal assemblages and stable isotopes. In: Contributions to the Micropaleontology and Paleoceanography of the Northern North Atlantic, Vol. 5, pp. 83–100.

Bauch, H.A., Erlenkeuser, H., Spielhagen, R.F., Struck, U., Matthiessen, J., Thiede, J., Heinemeier, J., 2001. A multiproxy reconstruction of the evolution of deep and surface waters in the subarctic Nordic seas over the last 30,000yr. Quat. Sci. Rev. 20, 659–678.

Bennike, O., Weidick, A., 2001. Late Quaternary history around Nioghalvfjerdsfjorden and Jøkelbugten, North-East Greenland. Boreas 30, 205–227.

Boyer, T.P., Garcia, H., Locarnini, R.A., Ricardo, A., Zweng, M.M., Mishonov, A.V., Reagan, J.R., Weathers, K.A., Baranova, O.K., Seidov, D., Smolyar, I.V., 2018. World Ocean Atlas 2018, NOAA National Centers for Environmental Information [Data Set]. available at: https://accession.nodc.noaa.gov/NCEI-WOA18.

Boyle, E.A., Keigwin, L., 1987. North Atlantic thermohaline circulation during the past 20,000 years linked to high-latitude surface temperature. Nature 330, 35–40.

Brendryen, J., Haflidason, H., Yokoyama, Y., Haaga, K.A., Hannisdal, B., 2020. Eurasian Ice Sheet collapse was a major source of Meltwater Pulse 1A 14,600 years ago. Nat. Geosci. 13, 363–368.

Cabedo-Sanz, P., Belt, S.T., Jennings, A.E., Andrews, J.T., Geirsdóttir, Á., 2016. Variability in drift ice export from the Arctic Ocean to the North Icelandic Shelf over the last 8000 years: a multi-proxy evaluation. Quat. Sci. Rev. 146, 99–115.

Cage, A.G., Pieńkowski, A.J., Jennings, A., Knudsen, K.L., Seidenkrantz, M.-S., 2021. Comparative analysis of six common foraminiferal species of the genera Cassidulina, Paracassidulina, and Islandiella from the Arctic–North Atlantic domain. J. Micropalaeontol. 40, 37–60.

Caralp, M.H., 1989. Size and morphology of the benthic foraminifer Melonis barleeanum; relationships with marine organic matter. J. Foram. Res. 19, 235–245.

Carlson, A.E., Clark, P.U., 2012. Ice sheet sources of sea level rise and freshwater discharge during the last deglaciation. Rev. Geophys. 50, RG4007.

Carlson, A.E., Stoner, J.S., Donnelly, J.P., Hillaire-Marcel, C., 2008. Response of the southern Greenland Ice Sheet during the last two deglaciations. Geology 36, 359–362.

Cofaigh, C.Ó., Dowdeswell, J.A., Evans, J., Kenyon, N.H., Taylor, J., Mienert, J., Wilken, M., 2004. Timing and significance of glacially influenced mass-wasting in the submarine channels of the Greenland Basin. Mar. Geol. 207, 39–54.

Cofaigh, Ó., Dowdeswell, J., Jennings, A., Hogan, K., Kilfeather, A., Hiemstra, J., Noormets, R., Evans, J., McCarthy, D., Andrews, J., 2013. An extensive and dynamic ice sheet on the West Greenland shelf during the last glacial cycle. Geology 41, 219–222.

Corliss, B.H., 1991. Morphology and microhabitat preferences of benthic foraminifera from the Northwest Atlantic Ocean. Mar. Micropaleontol. 17, 195–236.

Davies, J., Mathiasen, A.M., Kristiansen, K., Hansen, K.E., Wacker, L., Alstrup, A.K.O., Munk, O.L., Pearce, C., Seidenkrantz, M.-S., 2022. Linkages between ocean circulation and the Northeast Greenland Ice Stream in the early Holocene. Quat. Sci. Rev. 286 https://doi.org/10.1016/j.quascirev.2022.107530.

de Steur, L., Hansen, E., Mauritzen, C., Beszczynska-Möller, A., Fahrbach, E., 2014. Impact of recirculation on the East Greenland current in Fram Strait: results from moored current meter measurements between 1997 and 2009. Deep-Sea Res. I Oceanogr. Res. Pap. 92, 26–40.

de Vernal, A., Hillaire-Marcel, C., Darby, D.A., 2005. Variability of sea ice cover in the Chukchi Sea (western Arctic Ocean) during the Holocene. Paleoceanography 20, PA4018.

Deschamps, P., Durand, N., Bard, E., Hamelin, B., Camoin, G., Thomas, A.L., Henderson, G.M., Okuno, J., Yokoyama, Y., 2012. Ice-sheet collapse and sea-level rise at the Bolling warming 14,600 years ago. Nature 483, 559–564.

El bani Altuna, N., Ezat, M.M., Greaves, M., Rasmussen, T.L., 2021. Millennial-scale changes in bottom water temperature and water mass exchange through the fram strait 79°N, 63-13 ka. Paleoceanogr. Paleoclimatol. 36.

Evans, J., Dowdeswell, J.A., Grobe, H., Niessen, F., Stein, R., Hubberten, H.W., Whittington, R.J., 2002. Late Quaternary sedimentation in Kejser Franz Joseph Fjord and the continental margin of East Greenland. Geol. Soc. Lond., Spec. Publ. 203, 149–179.

Evans, J., Cofaigh, Ó., Dowdeswell, J.A., Wadhams, P., 2009. Marine geophysical evidence for former expansion and flow of the Greenland Ice Sheet across the north-east Greenland continental shelf. J. Quat. Sci. 24, 279–293.

Ezat, M.M., Rasmussen, T.L., Groeneveld, J., 2014. Persistent intermediate water warming during cold stadials in the southeastern Nordic seas during the past 65 ky. Geology 42, 663–666.

Ezat, M.M., Rasmussen, T.L., Hain, M.P., Greaves, M., James, W.B., Rae, J.W.B., Zamelczyk, K., Marchitto, T.M., Szidat, S., Skinner, L.C., 2021. Deep ocean storage of heat and CO2 in the Fram Strait, Arctic Ocean during the last glacial period. Paleoceanogr. Paleoclimatol. 36 https://doi.org/10.1029/2021PA004216 e2021PA004216.

Fairbanks, R.G., 1989. A 17,000-year glacio-eustatic sea level record: influence of glacial melting rates on the Younger Dryas event and deep-ocean circulation. Nature 342, 637–642.

Fieg, K., Gerdes, R., Fahrbach, E., Beszczynska-Möller, A., Schauer, U., 2010. Simulation of oceanic volume transports through Fram Strait 1995–2005. Ocean Dyn. 60, 491–502.

Fontanier, C., Jorissen, F., Licari, L., Alexandre, A., Anschutz, P., Carbonel, P., 2002. Live benthic foraminiferal faunas from the Bay of Biscay: faunal density, composition, and microhabitats. Deep-Sea Res. I Oceanogr. Res. Pap. 49, 751–785.

Fronval, T., Jansen, E., 1997. Eemian and early Weichselian (140–60 ka) paleoceanography and paleoclimate in the Nordic seas with comparisons to Holocene conditions. Paleoceanography 12, 443–462.

Greco, M., Jonkers, L., Kretschmer, K., Bijma, J., Kucera, M., 2019. Depth habitat of the planktonic foraminifera *Neogloboquadrina pachyderma* in the northern high latitudes explained by sea-ice and chlorophyll concentrations. Biogeosciences 16, 3425–3437.

Grootes, P.M., Stuiver, M., White, J., Johnsen, S., Jouzel, J., 1993. Comparison of oxygen isotope records from the GISP2 and GRIP Greenland ice cores. Nature 366, 552–554.

Haake, F.W., Pflaumann, U., 1989. Late Pleistocene foraminiferal stratigraphy on the Vøring plateau, Norwegian Sea. Boreas 18, 343–356.

Hald, M., Korsun, S., 1997. Distribution of modern benthic foraminifera from fjords of Svalbard, European Arctic. J. Foram. Res. 27, 101–122.

Hald, M., Steinsund, P.I., 1992. Distribution of surface sediment benthic foraminifera in the southwestern Barents Sea. J. Foram. Res. 22, 347–362.
Hald, M., Steinsund, P., 1996. Benthic foraminifera and carbonate dissolution in the surface sediments of the Barents and Kara Seas. Ber. Polarforsch. 212, 285–307.
Hald, M., Vorren, T.O., 1987. Foraminiferal stratigraphy and environment of late Weichselian deposits on the continental shelf off Troms, northern Norway. Mar. Micropaleontol. 12, 129–160.
Hald, M., Steinsund, P.I., Dokken, T., Korsun, S., Polyak, L., Aspeli, R., 1994. Recent and Late Quaternary Distribution of Elphidium Excavatumf. Clavatumin Arctic Seas. Cushman Foundation for Foraminiferal Research, p. 141.
Hattermann, T., Isachsen, P.E., von Appen, W.J., Albretsen, J., Sundfjord, A., 2016. Eddy-driven recirculation of Atlantic water in Fram Strait. Geophys. Res. Lett. 43, 3406–3414.
Håvik, L., Pickart, R.S., Våge, K., Torres, D., Thurnherr, A.M., Beszczynska-Möller, A., Walczowski, W., von Appen, W.J., 2017. Evolution of the East Greenland current from Fram Strait to Denmark Strait: synoptic measurements from summer 2012. J. Geophys. Res. Oceans 122, 1974–1994.
Heaton, T.J., Köhler, P., Butzin, M., Bard, E., Reimer, R.W., Austin, W.E., Ramsey, C.B., Grootes, P.M., Hughen, K.A., Kromer, B., 2020. Marine20—the marine radiocarbon age calibration curve (0–55,000 cal BP). Radiocarbon 62, 779–820.
Husum, K., Hald, M., 2012. Arctic planktic foraminiferal assemblages: Implications for subsurface temperature reconstructions. Mar. Micropaleontol. 96–97, 38–47.
Jackson, R., Andreasen, N., Oksman, M., Andersen, T.J., Pearce, C., Seidenkrantz, M.-S., Ribeiro, S., 2022. Marine conditions and development of the Sirius Water polynya on the North-East Greenland shelf during the Younger Dryas-Holocene. Quat. Sci. Rev. 291 https://doi.org/10.1016/j.quascirev.2022.107647.
Jeansson, E., Jutterström, S., Rudels, B., Anderson, L.G., Olsson, K.A., Jones, E.P., Smethie Jr., W.M., Swift, J.H., 2008. Sources to the East Greenland Current and its contribution to the Denmark Strait Overflow. Prog. Oceanogr. 78, 12–28.
Jennings, A.E., Helgadottir, G., 1994. Foraminiferal Assemblages from the Fjords and Shelf of Eastern Greenland. J Foramin Res 24, 123–144.
Jennings, A.E., Weiner, N.J., 1996. Environmental change in eastern Greenland during the last 1300 years: evidence from foraminifera and lithofacies in Nansen Fjord, 68 degrees N. Holocene 6, 179–191.
Jennings, A.E., Weiner, N.J., Helgadottir, G., Andrews, J.T., 2004. Modern foraminiferal faunas of the southwestern to northern Iceland shelf: oceanographic and environmental controls. J. Foram. Res. 34, 180–207.
Jessen, S.P., Rasmussen, T.L., Nielsen, T., Solheim, A., 2010. A new late Weichselian and Holocene marine chronology for the western Svalbard slope 30,000–0 cal years BP. Quat. Sci. Rev. 29, 1301–1312.
Johannessen, O.M., 1986. Brief Overview of the Physical Oceanography, The Nordic Seas. Springer, pp. 103–128.
Joughin, I., Fahnestock, M., MacAyeal, D., Bamber, J.L., Gogineni, P., 2001. Observation and analysis of ice flow in the largest Greenland ice stream. J. Geophys. Res.-Atmos. 106, 34021–34034.
Knies, J., Stein, R., 1998. New aspects of organic carbon deposition and its paleoceanographic implications along the Northern Barents Sea Margin during the last 30,000 years. Paleoceanography 13, 384–394.
Knudsen, K., Jiang, H., Jansen, E., Eiríksson, J., Heinemeier, J., Seidenkrantz, M.-S., 2004. Environmental changes off North Iceland during the deglaciation and the Holocene: foraminifera, diatoms and stable isotopes. Mar. Micropaleontol. 50, 273–305.
Knudsen, K.L., Stabell, B., Seidenkrantz, M.-S., EirÍKsson, J., Blake, W., 2008. Deglacial and Holocene conditions in northernmost Baffin Bay: sediments, foraminifera, diatoms and stable isotopes. Boreas 37, 346–376.
Koç, N., Jansen, E., Haflidason, H., 1993. Paleoceanographic reconstructions of surface ocean conditions in the Greenland, Iceland and Norwegian seas through the last 14 ka based on diatoms. Quat. Sci. Rev. 12, 115–140.
Korsun, S., Hald, M., 1998. Modern benthic foraminifera off Novaya Zemlya tidewater glaciers, Russian Arctic. Arct. Alp. Res. 30, 61–77.
Korsun, S., Polyak, L., 1989. Distribution of benthic foraminiferal morphogroups in the Barents Sea. Okeanologiya 29, 838–844.
Kristensen, D.K., Rasmussen, T.L., Koç, N., 2013. Palaeoceanographic changes in the northern Barents Sea during the last 16 000 years – new constraints on the last deglaciation of the Svalbard-Barents Sea Ice Sheet. Boreas 42, 798–813.
Łącka, M., Zajączkowski, M., 2016. Does the recent pool of benthic foraminiferal tests in fjordic surface sediments reflect interannual environmental changes? The resolution limit of the foraminiferal record. Ann. Soc. Geol. Pol. 59–71. https://doi.org/10.14241/asgp.12015.14019.
Łącka, M., Zajączkowski, M., Forwick, M., Szczuciński, W., 2015. Late Weichselian and Holocene palaeoceanography of Storfjordrenna, southern Svalbard. Clim. Past 11, 587–603.
Łącka, M., Cao, M., Rosell-Melé, A., Pawłowska, J., Kucharska, M., Forwick, M., Zajączkowski, M., 2019. Postglacial paleoceanography of the western Barents Sea: Implications for alkenone-based sea surface temperatures and primary productivity. Quat. Sci. Rev. 224, 105973–105986.
Łącka, M., Michalska, D., Pawlowska, J., Szymanska, N., Szczucinski, W., Forwick, M., Zajaczkowski, M., 2020. Multiproxy paleoceanographic study from the western Barents Sea reveals dramatic Younger Dryas onset followed by oscillatory warming trend. Sci. Rep. 10, 15667–15674.
Larsen, N.K., Kjær, K.H., Funder, S., Möller, P., van der Meer, J.J., Schomacker, A., Linge, H., Darby, D.A., 2010. Late Quaternary glaciation history of northernmost Greenland–evidence of shelf-based ice. Quat. Sci. Rev. 29, 3399–3414.
Larsen, N.K., Levy, L.B., Carlson, A.E., Buizert, C., Olsen, J., Strunk, A., Bjork, A.A., Skov, D.S., 2018. Instability of the Northeast Greenland Ice Stream over the last 45,000 years. Nat. Commun. 9, 1872.
Lekens, W., Sejrup, H.P., Haflidason, H., Petersen, G., Hjelstuen, B., Knorr, G., 2005. Laminated sediments preceding Heinrich event 1 in the Northern North Sea and Southern Norwegian Sea: origin, processes and regional linkage. Mar. Geol. 216, 27–50.
Loeblich Jr., A.R., Tappan, H., 2015. Foraminiferal Genera and their Classification. Springer.
Lubinski, D.J., Polyak, L., Forman, S.L., 2001. Freshwater and Atlantic water inflows to the deep northern Barents and Kara seas since ca 13 14Cka. Quat. Sci. Rev. 20, 1851–1879.
Mackensen, A., Sejrup, H., Jansen, E., 1985. The distribution of living benthic foraminifera on the continental slope and rise off Southwest Norway. Mar. Micropaleontol. 9, 275–306.
Mangerud, J., Bolstad, M., Elgersma, A., Helliksen, D., Landvik, J.Y., Lønne, I., Lycke, A. K., Salvigsen, O., Sandahl, T., Svendsen, J.I., 1992. The last glacial maximum on Spitsbergen, Svalbard. Quat. Res. 38, 1–31.
Mangerud, J., Bondevik, S., Gulliksen, S., Karin Hufthammer, A., Høisæter, T., 2006. Marine 14C reservoir ages for 19th century whales and molluscs from the North Atlantic. Quat. Sci. Rev. 25, 3228–3245.
McManus, J.F., Francois, R., Gherardi, J.M., Keigwin, L.D., Brown-Leger, S., 2004. Collapse and rapid resumption of Atlantic meridional circulation linked to deglacial climate changes. Nature 428, 834–837.
Mienert, J., Andrews, J.T., Milliman, J.D., 1992. The East Greenland continental margin (65 N) since the last deglaciation: changes in seafloor properties and ocean circulation. Mar. Geol. 106, 217–238.
Möller, P., Larsen, N.K., Kjær, K.H., Funder, S., Schomacker, A., Linge, H., Fabel, D., 2010. Early to middle Holocene valley glaciations on northernmost Greenland. Quat. Sci. Rev. 29, 3379–3398.
Moros, M., Kuijpers, A., Snowball, I., Lassen, S., Bäckström, D., Gingele, F., McManus, J., 2002. Were glacial iceberg surges in the North Atlantic triggered by climatic warming? Mar. Geol. 192, 393–417.
Mudie, P., Keen, C., Hardy, I., Vilks, G., 1984. Multivariate analysis and quantitative paleoecology of benthic foraminifera in surface and Late Quaternary shelf sediments, northern Canada. Mar. Micropaleontol. 8, 283–313.
Müller, J., Massé, G., Stein, R., Belt, S.T., 2009. Variability of sea-ice conditions in the Fram Strait over the past 30,000 years. Nat. Geosci. 2, 772–776.
Müller, J., Werner, K., Stein, R., Fahl, K., Moros, M., Jansen, E., 2012. Holocene cooling culminates in sea ice oscillations in Fram Strait. Quat. Sci. Rev. 47, 1–14.
Nam, S.-I., Stein, R., Grobe, H., Hubberten, H., 1995. Late Quaternary glacial-interglacial changes in sediment composition at the East Greenland continental margin and their paleoceanographic implications. Mar. Geol. 122, 243–262.
Nørgaard-Pedersen, N., Spielhagen, R.F., Erlenkeuser, H., Grootes, P.M., Heinemeier, J., Knies, J., 2003. Arctic Ocean during the last Glacial Maximum: Atlantic and polar domains of surface water mass distribution and ice cover. Paleoceanography 18, 1063.
Pados, T., Spielhagen, R.F., 2014. Species distribution and depth habitat of recent planktic foraminifera in Fram Strait, Arctic Ocean. Polar Res. 33, 22483.
Pados-Dibattista, T., Pearce, C., Detlef, H., Bendtsen, J., Seidenkrantz, M.-S., 2022. Holocene palaeoceanography of the Northeast Greenland shelf. Clim. Past 18, 103–127.
Paquette, R.G., Bourke, R.H., Newton, J.F., Perdue, W.F., 1985. The East Greenland polar front in autumn. J. Geophys. Res. Oceans 90, 4866–4882.
Piotrowski, A.M., Goldstein, S.L., Hemming, S.R., Fairbanks, R.G., 2005. Temporal relationships of carbon cycling and ocean circulation at glacial boundaries. Science 307, 1933–1938.
Poole, D., Dokken, T., Hald, M., Polyak, L., 1994. Stable Isotope Fractionation in Recent Benthic Foraminifera from the Barents and Kara Seas. PhD. University of Bergen, p. 20.
Rasmussen, T.L., Thomsen, E., 2008. Warm Atlantic surface water inflow to the Nordic seas 34-10 calibrated ka B.P. Paleoceanography 23, PA1201.
Rasmussen, T.L., Thomsen, E., van Weering, T.C.E., Labeyrie, L., 1996. Rapid changes in surface and deep water conditions at the Faeroe margin during the last 58,000 years. Paleoceanography 11, 757–771.
Rasmussen, T.L., Thomsen, E., Ślubowska, M.A., Jessen, S., Solheim, A., Koç, N., 2007. Paleoceanographic evolution of the SW Svalbard margin (76°N) since 20,000 14C yr BP. Quat. Res. 67, 100–114.
Rasmussen, S.O., Abbott, P.M., Blunier, T., Bourne, A.J., Brook, E., Buchardt, S.L., Buizert, C., Chappellaz, J., Clausen, H.B., Cook, E., Dahl-Jensen, D., Davies, S.M., Guillevic, M., Kipfstuhl, S., Laepple, T., Seierstad, I.K., Severinghaus, J.P., Steffensen, J.P., Stowasser, C., Svensson, A., Vallelonga, P., Vinther, B.M., Wilhelms, F., Winstrup, M., 2013. A first chronology for the North Greenland Eemian Ice Drilling (NEEM) ice core. Clim. Past 9, 2713–2730.
Rasmussen, T.L., Thomsen, E., Skirbekk, K., Slubowska-Woldengen, M., Klitgaard Kristensen, D., Koç, N., 2014. Spatial and temporal distribution of Holocene temperature maxima in the northern Nordic seas: interplay of Atlantic-, Arctic- and polar water masses. Quat. Sci. Rev. 92, 280–291.
Rasmussen, T.L., Pearce, C., Andresen, K.J., Nielsen, T., Seidenkrantz, M.-S., 2022. Northeast Greenland: ice-free shelf edge at 79.4°N around the Last Glacial Maximum 25.5–17.5 ka. Boreas. https://doi.org/10.1111/bor.12593.
Risebrobakken, B., Dokken, T., Smedsrud, L.H., Andersson, C., Jansen, E., Moros, M., Ivanova, E.V., 2011. Early Holocene temperature variability in the Nordic Seas: the role of oceanic heat advection versus changes in orbital forcing. Paleoceanography 26, PA4206.
Rørvik, K.-L., Laberg, J., Hald, M., Ravna, E., Vorren, T., 2010. Behavior of the northwestern part of the Fennoscandian Ice Sheet during the last Glacial Maximum–a response to external forcing. Quat. Sci. Rev. 29, 2224–2237.

Rudels, B., 1989. The formation of polar surface water, the ice export and the exchanges through the Fram Strait. Prog. Oceanogr. 22, 205–248.
Rudels, B., Quadfasel, D., 1991. Convection and deep water formation in the Arctic Ocean-Greenland Sea system. J. Mar. Syst. 2, 435–450.
Rudels, B., Fahrbach, E., Meincke, J., Budeus, G., Eriksson, P., 2002. The East Greenland current and its contribution to the Denmark Strait overflow. ICES J. Mar. Sci. 59, 1133–1154.
Rudels, B., Björk, G., Nilsson, J., Winsor, P., Lake, I., Nohr, C., 2005. The interaction between waters from the Arctic Ocean and the Nordic Seas north of Fram Strait and along the East Greenland current: results from the Arctic Ocean-02 Oden expedition. J. Mar. Syst. 55, 1–30.
Rudels, B., Korhonen, M., Budéus, G., Beszczynska-Möller, A., Schauer, U., Nummelin, A., Quadfasel, D., Valdimarsson, H.i., 2012. The East Greenland current and its impacts on the Nordic Seas: observed trends in the past decade. ICES J. Mar. Sci. 69, 841–851.
Sarnthein, M., Jansen, E., Weinelt, M., Arnold, M., Duplessy, J.C., Erlenkeuser, H., Flatøy, A., Johannessen, G., Johannessen, T., Jung, S., 1995. Variations in Atlantic surface ocean paleoceanography, 50°–80° N: a time-slice record of the last 30,000 years. Paleoceanography 10, 1063–1094.
Schaffer, J., von Appen, W.-J., Dodd, P.A., Hofstede, C., Mayer, C., de Steur, L., Kanzow, T., 2017. Warm water pathways toward Nioghalvfjerdsfjorden Glacier, Northeast Greenland. J. Geophys. Res. Oceans 122, 4004–4020.
Schaffer, J., Kanzow, T., von Appen, W.-J., von Albedyll, L., Arndt, J.E., Roberts, D.H., 2020. Bathymetry constrains ocean heat supply to Greenland's largest glacier tongue. Nat. Geosci. 13, 227–231.
Scott, D.B., Mudie, P.J., Vilks, G., Younger, D.C., 1984. Latest Pleistocene—Holocene paleoceanographic trends on the continental margin of eastern Canada: foraminiferal, dinoflagellate and pollen evidence. Mar. Micropaleontol. 9, 181–218.
Seidenkrantz, M.-S., 1995. Cassidulina teretis Tappan and Cassidulina neoteretis new species (Foraminifera): stratigraphic markers for deep sea and outer shelf areas. J. Micropalaeontol. 14, 145–157.
Seidenkrantz, M.-S., 2013. Benthic foraminifera as palaeo sea-ice indicators in the subarctic realm – examples from the Labrador Sea–Baffin Bay region. Quat. Sci. Rev. 79, 135–144.
Sejrup, H.-P., Fjaeran, T., Hald, M., Beck, L., Hagen, J., Miljeteig, I., Morvik, I., Norvik, O., 1981. Benthonic foraminifera in surface samples from the Norwegian continental margin between 62 degrees N and 65 degrees N. J. Foram. Res. 11, 277–295.
Sheldon, C., Jennings, A., Andrews, J.T., Cofaigh, Ó., Hogan, K., Dowdeswell, J.A., Seidenkrantz, M.-S., 2016. Ice stream retreat following the LGM and onset of the West Greenland current in Uummannaq Trough, West Greenland. Quat. Sci. Rev. 147, 27–46.
Simstich, J., Sarnthein, M., Erlenkeuser, H., 2003. Paired δ18O signals of Neogloboquadrina pachyderma (s) and Turborotalita quinqueloba show thermal stratification structure in Nordic Seas. Mar. Micropaleontol. 48, 107–125.
Ślubowska, M.A., Koç, N., Rasmussen, T.L., Klitgaard-Kristensen, D., 2005. Changes in the flow of Atlantic water into the Arctic Ocean since the last deglaciation: evidence from the northern Svalbard continental margin, 80°N. Paleoceanography 20, PA4014.
Ślubowska-Woldengen, M., Rasmussen, T.L., Koç, N., Klitgaard-Kristensen, D., Nilsen, F., Solheim, A., 2007. Advection of Atlantic Water to the western and northern Svalbard shelf since 17,500calyr BP. Quat. Sci. Rev. 26, 463–478.
Spielhagen, R.F., Mackensen, A., 2021. Upper Ocean variability off NE Greenland (79°N) since the last glacial maximum reconstructed from stable isotopes in planktic foraminifer morphotypes. Quat. Sci. Rev. 265, 107070–107082.
Steinsund, P., 1994. Benthic Foraminifera in Surface Sediments of the Barents and Kara Seas: Modern and Late Quaternary Applications. University of Tromsø, Tromsø (111 pp).
Stuiver, M., Reimer, P.J., Reimer, R.W., 2022. CALIB 8.2 [WWW program]. at. http://calib.org. accessed 2022–2–25.
Syring, N., Lloyd, J.M., Stein, R., Fahl, K., Roberts, D.H., Callard, L., O'Cofaigh, C., 2020a. Holocene interactions between Glacier Retreat, sea ice formation, and Atlantic Water advection at the Inner Northeast Greenland continental shelf. Paleoceanogr. Paleoclimatol. 35 https://doi.org/10.1029/2020PA004019.
Syring, N., Stein, R., Fahl, K., Vahlenkamp, M., Zehnich, M., Spielhagen, R.F., Niessen, F., 2020b. Holocene changes in sea-ice cover and polynya formation along the eastern North Greenland shelf: New insights from biomarker records. Quat. Sci. Rev. 231, 106173–106188.
Syvitski, J.P.M., Andrews, J.T., Dowdeswell, J.A., 1996. Sediment deposition in an iceberg-dominated glacimarine environment, East Greenland: basin fill implications. Glob. Planet. Chang. 12, 251–270.
Sztybor, K., Rasmussen, T.L., 2017. Late glacial and deglacial palaeoceanographic changes at Vestnesa Ridge, Fram Strait: methane seep versus non-seep environments. Palaeogeogr. Palaeoclimatol. Palaeoecol. 476, 77–89.
Telesiński, M.M., Spielhagen, R.F., Bauch, H.A., 2014. Water mass evolution of the Greenland Sea since late glacial times. Clim. Past 10, 123–136.
Telesiński, M.M., Przytarska, J.E., Sternal, B., Forwick, M., Szczuciński, W., Łącka, M., Zajączkowski, M., 2018. Palaeoceanographic evolution of the SW Svalbard shelf over the last 14 000 years. Boreas 47, 410–422.
Telesiński, M.M., Łącka, M., Kujawa, A., Zajączkowski, M., 2022. The significance of Atlantic Water routing in the Nordic Seas: the Holocene perspective. The Holocene. https://doi.org/10.1177/09596836221106974, 09596836221106974.
Volkmann, R., 2000. Planktic foraminifers in the outer Laptev Sea and the Fram Strait—modern distribution and ecology. J. Foram. Res. 30, 157–176.
Vorren, T.O., Kristoffersen, Y., 1986. Late Quaternary glaciation in the South-Western Barents Sea. Boreas 15, 51–59.
Werner, K., Spielhagen, R.F., Bauch, D., Hass, H.C., Kandiano, E., 2013. Atlantic Water advection versus sea-ice advances in the eastern Fram Strait during the last 9 ka: multiproxy evidence for a two-phase Holocene. Paleoceanography 28, 283–295.
Werner, K., Müller, J., Husum, K., Spielhagen, R.F., Kandiano, E.S., Polyak, L., 2016. Holocene Sea subsurface and surface water masses in the Fram Strait – comparisons of temperature and sea-ice reconstructions. Quat. Sci. Rev. 147, 194–209.
Wollenburg, J.E., Kuhnt, W., 2000. The response of benthic foraminifers to carbon flux and primary production in the Arctic Ocean. Mar. Micropaleontol. 40, 189–231.
Wollenburg, J.E., Mackensen, A., 1998. Living benthic foraminifers from the Central Arctic Ocean: faunal composition, standing stock and diversity. Mar. Micropaleontol. 34, 153–185.
Zehnich, M., Spielhagen, R.F., Bauch, H.A., Forwick, M., Hass, H.C., Palme, T., Stein, R., Syring, N., 2020. Environmental variability off NE Greenland (western Fram Strait) during the past 10,600 years. The Holocene 30, 1752–1766.